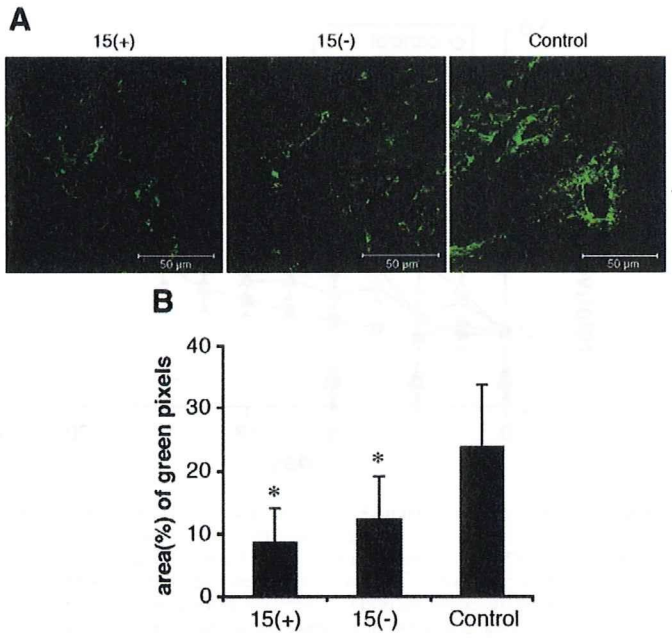

Fig. 6. Antiangiogenic effect of expressed sFlt-1 in BxPC3 tumor bearing mice. Tumor microvessels were detected by CD31 (PECAM1) antibody staining of tumor cryosections 20 days after therapy. (A) Representative CD31 immunostaining images. (B) Quantitative analysis of microvessel density in tumor cryosections. The results represent a percentage area of green pixels per image. Seven images were taken from each tumor tissue, from 3 mice, mean ± s.d. $^{*}P<0.05$ compared to control group.

Science and Technology Agency (JST) as well as by Grants-in-Aid for Young Scientists (A). We express our appreciation to Prof. M. Shibuya (Tokyo Medical and Dental University) for providing pVL 1393 baculovirus vector pDNA encoding human sFlt-1. We thank Ms. S. Ogura (The University of Tokyo) for her technical assistance.

References

[1] A. Harada, K. Kataoka, Formation of polycation complex micelles in an aqueous milieu from a pair of oppositely-charged block copolymers with poly(ethylene glycol) segments, Macromolecules 28 (15) (1995) 5294–5299.
[2] S. Katayose, K. Kataoka, Water-soluble polyion complex associates of DNA and poly(ethylene glycol)-poly(L-lysine) block copolymer, Bioconjug. Chem. 8 (5) (1997) 702–707.
[3] M. Harada-Shiba, K. Yamauchi, A. Harada, I. Takamisawa, K. Shimokado, K. Kataoka, Polyion complex micelles as vectors in gene therapy — pharmacokinetics and in vivo gene transfer, Gene Ther. 9 (6) (2002) 407–414.
[4] M. Laus, K. Sparnacci, B. Ensoli, S.O. Buttò, A. Caputo, I. Mantovani, G. Zuccheri, B. Samorì, L. Tondelli, Complex associates of plasmid DNA and a novel class of block copolymers with PEG and cationic segments as new vectors for gene delivery, J. Biomater. Sci. Polym. Ed. 12 (2) (2001) 209–228.
[5] C.H. Ahn, S.Y. Chae, Y.H. Bae, S.W. Kim, Synthesis of biodegradable multi-block copolymers of poly(L-lysine) and poly(ethylene glycol) as a non-viral gene carrier, J. Control. Release 97 (3) (2004) 567–574.
[6] Y. Wang, C.Y. Ke, B.C. Weijie, S.Q. Liu, S.H. Goh, Y.Y. Yang, The self-assembly of biodegradable cationic polymer micelles as vectors for gene transfection, Biomaterials 28 (35) (2007) 5358–5368.
[7] Y.R. Choi, S.Y. Chae, C.H. Ahn, M. Lee, S. Oh, Y. Byun, B.D. Rhee, K.S. Ko, Development of polymeric gene delivery carriers: PEGylated copolymers of L-lysine and L-phenylalanine, J. Drug Target. 15 (6) (2007) 391–398.
[8] K. Itaka, K. Yamauchi, A. Harada, K. Nakamura, H. Kawaguchi, K. Kataoka, Polyion complex micelles from plasmid DNA and poly(ethylene glycol)-poly(L-lysine) block copolymer as serum-tolerable polyplex system: physicochemical properties of micelles relevant to gene transfection efficiency, Biomaterials 24 (24) (2003) 4495–4506.
[9] S. Mishra, P. Webster, M.E. Davis, PEGylation significantly affects cellular uptake and intracellular trafficking of non-viral gene delivery particles, Eur. J. Cell Biol. 83 (3) (2004) 97–111.
[10] A.M. Funhoff, S. Monge, R. Teeuwen, G.A. Koning, N.M. Schuurmans-Nieuwenbroek, D.J. Crommelin, D.M. Haddleton, W.E. Hennink, C.F. van Nostrum, PEG shielded polymeric double-layered micelles for gene delivery, J. Control. Release 102 (3) (2005) 711–724.
[11] H.K. de Wolf, C.J. Snel, F.J. Verbaan, R.M. Schiffelers, W.E. Hennink, G. Storm, Effect of cationic carriers on the pharmacokinetics and tumor localization of nucleic acids after intravenous administration, Int. J. Pharm. 331 (2) (2007) 167–175.
[12] K. Miyata, Y. Kakizawa, N. Nishiyama, A. Harada, Y. Yamasaki, H. Koyama, K. Kataoka, Block catiomer polyplexes with regulated densities of charge and disulfide cross-linking directed to enhance gene expression, J. Am. Chem. Soc. 126 (8) (2004) 2355–2361.
[13] K. Miyata, Y. Kakizawa, N. Nishiyama, Y. Yamasaki, T. Watanabe, M. Kohara, K. Kataoka, Freeze-dried formulations for in vivo gene delivery of PEGylated polyplex micelles with disulfide crosslinked cores to the liver, J. Control. Release 109 (1–3) (2005) 15–23.
[14] M. Oba, S. Fukushima, N. Kanayama, K. Aoyagi, N. Nishiyama, H. Koyama, K. Kataoka, Cyclic RGD peptide-conjugated polyplex micelles as a targetable gene delivery system directed to cells possessing $\alpha_v\beta_3$ and $\alpha_v\beta_5$ integrins, Bioconjug. Chem. 18 (5) (2007) 1415–1423.
[15] M. Oba, K. Aoyagi, K. Miyata, Y. Matsumoto, K. Itaka, N. Nishiyama, Y. Yamasaki, H. Koyama, K. Kataoka, Polyplex Micelles with cyclic RGD peptide ligands and disulfide cross-links directing to the enhanced transfection via controlled intracellular trafficking, Mol. Pharmaceutics 5 (6) (2008) 1080–1092.
[16] M.D. Pierschbacher, E. Ruoslahti, Cell attachment activity of fibronectin can be duplicated by small synthetic fragments of the molecule, Nature 309 (5963) (1984) 30–33.
[17] R. Haubner, R. Gratias, B. Diefenbach, S.L. Goodman, A. Jonczyk, H. Kessler, Structural and functional aspects of RGD-containing cyclic pentapeptides as highly potent and selective integrin $\alpha_v\beta_3$ antagonists, J. Am. Chem. Soc. 118 (1996) 7461–7472.
[18] A. Erdreich-Epstein, H. Shimada, S. Groshen, M. Liu, L.S. Metelitsa, K.S. Kim, M.F. Stins, R.C. Seeger, D.L. Durden, Integrins alpha(v)beta3 and alpha(v)beta5 are expressed by endothelium of high-risk neuroblastoma and their inhibition is associated with increased endogenous ceramide, Cancer Res. 60 (3) (2000) 712–721.
[19] R.M. Schiffelers, A. Ansari, J. Xu, Q. Zhou, Q. Tang, G. Storm, G. Molema, P.Y. Lu, P.V. Scaria, M.C. Woodle, Cancer siRNA therapy by tumor selective delivery with ligand-targeted sterically stabilized nanoparticle, Nucleic Acids Res. 32 (19) (2004) e149.
[20] W.J. Kim, J.W. Yockman, M. Lee, J.H. Jeong, Y.H. Kim, S.W. Kim, Soluble Flt-1 gene delivery using PEI-g-PEG-RGD conjugate for anti-angiogenesis, J. Control. Release 106 (1–2) (2005) 224–234.
[21] W.J. Kim, J.W. Yockman, J.H. Jeong, L.V. Christensen, M. Lee, Y.H. Kim, S.W. Kim, Anti-angiogenic inhibition of tumor growth by systemic delivery of PEI-g-PEG-RGD/pCMV-sFlt-1 complexes in tumor-bearing mice, J. Control. Release 114 (3) (2006) 381–388.
[22] K. Temming, R.M. Schiffelers, G. Molema, R.J. Kok, RGD-based strategies for selective delivery of therapeutics and imaging agents to the tumor vasculature, Drug Resist. Updat. 8 (6) (2005) 381–402.
[23] K.A. Thomas, Vascular endothelial growth factor, a potent and selective angiogenic agent, J. Biol. Chem. 271 (2) (1996) 603–606.
[24] G. Breier, Functions of the VEGF/VEGF receptor system in the vascular system, Semin. Thromb. Hemost. 26 (5) (2000) 553–559.
[25] R.A. Brekken, P.E. Thorpe, VEGF-VEGF receptor complexes as markers of tumor vascular endothelium, J. Control. Release 74 (1–3) (2001) 173–181.
[26] A.L. Harris, Anti-angiogenesis therapy and strategies for integrating it with adjuvant therapy, Recent Results Cancer Res. 152 (1998) 341–352.
[27] N. Ferrara, VEGF as a therapeutic target in cancer, Oncology 69 (2005) 11–16.
[28] R.L. Kendall, G. Wang, K.A. Thomas, Identification of a natural soluble form of the vascular endothelial growth factor receptor, FLT-1, and its heterodimerization with KDR, Biochem. Biophys. Res. Commun. 226 (2) (1996) 324–328.
[29] H. Chen, U. Ikeda, M. Shimpo, Y. Maeda, M. Shibuya, K. Ozawa, K. Shimada, Inhibition of vascular endothelial growth factor activity by transfection with the soluble FLT-1 gene, J. Cardiovasc. Pharmacol. 36 (4) (2000) 498–502.
[30] M. Malecki, H. Trembacz, B. Szaniawska, M. Przybyszewska, P. Janik, Vascular endothelial growth factor and soluble FLT-1 receptor interactions and biological implications, Oncol. Rep. 14 (6) (2005) 1565–1569.
[31] C. Ye, C. Feng, S. Wang, K.Z. Wang, N. Huang, X. Liu, Y. Lin, M. Li, sFlt-1 gene therapy of follicular thyroid carcinoma, Endocrinology 145 (2) (2004) 817–822.
[32] Y. Hasumi, H. Mizukami, M. Urabe, T. Kohno, K. Takeuchi, A. Kume, M. Momoeda, H. Yoshikawa, T. Tsuruo, M. Shibuya, Y. Taketani, K. Ozawa, Soluble FLT-1 expression suppresses carcinomatous ascites in nude mice bearing ovarian cancer, Cancer Res. 62 (7) (2002) 2019–2023.
[33] G. Mahendra, S. Kumar, T. Isayeva, P.J. Mahasreshti, D.T. Curiel, C.R. Stockardt, W.E. Grizzle, V. Alapati, R. Singh, G.P. Siegal, S. Meleth, S. Ponnazhagan, Antiangiogenic cancer gene therapy by adeno-associated virus 2-mediated stable expression of the soluble FMS-like tyrosine kinase-1 receptor, Cancer Gene Ther. 12 (1) (2005) 26–34.
[34] Y. Takei, H. Mizukami, Y. Saga, I. Yoshimura, Y. Hasumi, T. Takayama, T. Kohno, T. Matsushita, T. Okada, A. Kume, M. Suzuki, K. Ozawa, Suppression of ovarian cancer by muscle-mediated expression of soluble VEGFR-1/Flt-1 using adeno-associated virus serotype 1-derived vector, Int. J. Cancer 120 (2) (2007) 278–284.
[35] S. Kommareddy, M. Amiji, Antiangiogenic gene therapy with systemically administered sFlt-1 plasmid DNA in engineered gelatin-based nanovectors, Cancer Gene Ther. 14 (5) (2007) 488–498.
[36] M.R. Kano, Y. Komuta, C. Iwata, M. Oka, Y.T. Shirai, Y. Morishita, Y. Ouchi, K. Kataoka, K. Miyazono, Comparison of the effects of the kinase inhibitors imatinib, sorafenib, and transforming growth factor-beta receptor inhibitor on extravasation of nanoparticles from neovasculature, Cancer Sci. 100 (1) (2009) 173–180.
[37] A. Harada, K. Kataoka, Formation of polyion complex micelles in an aqueous milieu from a pair of oppositely charged block copolymers with poly(ethylene glycol) segments, Macromolecules 28 (1995) 294–299.

Please cite this article as: Y. Vachutinsky, et al., Antiangiogenic gene therapy of experimental pancreatic tumor by sFlt-1 plasmid DNA carried by RGD-modified crosslinked polyplex mi..., J. Control. Release (2010), doi:10.1016/j.jconrel.2010.02.002

[38] P.K. Dubey, V. Mishra, S. Jain, S. Mahor, S.P. Vyas, Liposomes modified with cyclic RGD peptide for tumor targeting, J. Drug Target. 12 (5) (2004) 257–264.
[39] A.J. Schraa, R.J. Kok, H.E. Moorlag, E.J. Bos, J.H. Proost, D.K. Meijer, L.F. de Leij, G. Molema, Targeting of RGD-modified proteins to tumor vasculature: a pharmacokinetic and cellular distribution study, Int. J. Cancer 102 (5) (2002) 469–475.
[40] R.M. Schiffelers, G.A. Koning, T.L. ten Hagen, M.H. Fens, A.J. Schraa, A.P. Janssen, R.J. Kok, G. Molema, G. Storm, Anti-tumor efficacy of tumor vasculature-targeted liposomal doxorubicin, J. Control. Release 91 (1–2) (2003) 115–122.
[41] A. Mitra, J. Mulholland, A. Nan, E. McNeill, H. Ghandehari, B.R. Line, Targeting tumor angiogenic vasculature using polymer-RGD conjugates, J. Control. Release 102 (1) (2005) 191–201.
[42] D.C. Bibby, J.E. Talmadge, M.K. Dalal, S.G. Kurz, K.M. Chytil, S.E. Barry, D.G. Shand, M. Steiert, Pharmacokinetics and biodistribution of RGD-targeted doxorubicin-loaded nanoparticles in tumor-bearing mice, Int. J. Pharm. 293 (1–2) (2005) 281–290.

Please cite this article as: Y. Vachutinsky, et al., Antiangiogenic gene therapy of experimental pancreatic tumor by sFlt-1 plasmid DNA carried by RGD-modified crosslinked polyplex mi..., J. Control. Release (2010), doi:10.1016/j.jconrel.2010.02.002

molecular pharmaceutics

articles

Antiangiogenic Gene Therapy of Solid Tumor by Systemic Injection of Polyplex Micelles Loading Plasmid DNA Encoding Soluble Flt-1

Makoto Oba,[†] Yelena Vachutinsky,[‡] Kanjiro Miyata,[§] Mitsunobu R. Kano,[∥,⊥] Sorato Ikeda,[#] Nobuhiro Nishiyama,[*,§] Keiji Itaka,[§] Kohei Miyazono,[∥,⊥] Hiroyuki Koyama,[†] and Kazunori Kataoka[*,‡,§,∥,#]

Department of Clinical Vascular Regeneration, Graduate School of Medicine, The University of Tokyo, 7-3-1 Hongo, Bunkyo, Tokyo 113-8655, Japan, Department of Bioengineering, Graduate School of Engineering, The University of Tokyo, 7-3-1 Hongo, Bunkyo, Tokyo 113-8656, Japan, Center for Disease Biology and Integrative Medicine, Graduate School of Medicine, The University of Tokyo, 7-3-1 Hongo, Bunkyo, Tokyo 113-0033, Japan, Center for NanoBio Integration, The University of Tokyo, 7-3-1 Hongo, Bunkyo, Tokyo 113-8656, Japan, Department of Molecular Pathology, Graduate School of Medicine, The University of Tokyo, 7-3-1 Hongo, Bunkyo-ku, Tokyo 113-8655, Japan, and Department of Materials Engineering, Graduate School of Engineering, The University of Tokyo, 7-3-1 Hongo, Bunkyo, Tokyo 113-8656, Japan

Received September 14, 2009; Revised Manuscript Received January 8, 2010; Accepted February 23, 2010

Abstract: In this study, a polyplex micelle was developed as a potential formulation for antiangiogenic gene therapy of subcutaneous pancreatic tumor model. Poly(ethylene glycol)-poly(L-lysine) block copolymers (PEG-PLys) with thiol groups in the side chain of the PLys segment were synthesized and applied for preparation of disulfide cross-linked polyplex micelles through ion complexation with plasmid DNA (pDNA) encoding the soluble form of vascular endothelial growth factor (VEGF) receptor-1 (sFlt-1), which is a potent antiangiogenic molecule. Antitumor activity and gene expression of polyplex micelles with various cross-linking rates were evaluated in mice bearing subcutaneously xenografted BxPC3 cell line, derived from human pancreatic adenocarcinoma, and polyplex micelles with optimal cross-linking rate achieved effective suppression of tumor growth. Significant gene expression of this micelle was detected selectively in tumor tissue, and its antiangiogenic effect was confirmed by decreased vascular density inside the tumor. Therefore, the disulfide cross-linked polyplex micelle loading sFlt-1 pDNA has a great potential for antiangiogenic therapy against subcutaneous pancreatic tumor model by systemic application.

Keywords: Polymeric micelle; block copolymer; antiangiogenic tumor gene therapy; sFlt-1

Introduction

Antiangiogenic tumor gene therapy is an intensively studied approach to inhibit tumor growth by destructing its neo-vasculature formation.[1,2] Vascular endothelial growth factor (VEGF) is a major proangiogenic molecule, which stimulates angiogenesis via promoting endothelial prolifera-

* To whom correspondence should be addressed. K.K.: tel, +81-3-5841-7138; fax, +81-3-5841-7139; e-mail, kataoka@bmw.t.u-tokyo.ac.jp; The University of Tokyo, Department of Materials Engineering, 7-3-1 Hongo, Bunkyo-ku, Tokyo 113-8656, Japan. N.N.: tel, +81-3-5841-1430; fax, +81-5841-7139; e-mail, nishiyama@bmw.t.u-tokyo.ac.jp.

† Department of Clinical Vascular Regeneration, Graduate School of Medicine.

‡ Department of Bioengineering, Graduate School of Engineering.

§ Center for Disease Biology and Integrative Medicine, Graduate School of Medicine.

∥ Center for NanoBio Integration.

⊥ Department of Molecular Pathology, Graduate School of Medicine.

Department of Materials Engineering, Graduate School of Engineering.

10.1021/mp9002317 © 2010 American Chemical Society
Published on Web 02/23/2010

tion, survival, and migration. The soluble form of VEGF receptor-1 (fms-like tyrosine kinase-1: Flt-1) is a potent endogeneous molecule, which can be used for antiangiogenic therapy.[3,4] The sFlt-1 binds to VEGF with the same affinity and equivalent specificity as that of the original receptor,[5] however it inhibits its signal transduction.

Gene therapy is becoming a promising strategy to supply consecutive expression of antiangiogenic proteins over a period of time. Indeed, a number of studies have already demonstrated the potential of therapeutic genes encoding angiogenic inhibitors to suppress tumor growth.[6,7] The major challenge in systemic gene therapy, however, is a need for a safe and effective vector system that can deliver the gene to the target tissue and cells with no detrimental side effects. In terms of safety, nonviral gene vectors are gaining popularity over viral vectors, however, their intracellular delivery and transfection potential require further optimization. Recently, several reports were published on *in vivo* nonviral gene therapy utilizing sFlt-1 for inhibition of tumor angiogenesis.[8,9]

Based on these criteria, cross-linked polyplex micelles were designed and prepared through electrostatic interaction of thiolated poly(ethylene glycol)-poly(L-lysine) (PEG-PLys) block copolymers and plasmid DNA (pDNA) encoding sFlt-1. We have previously reported that disulfide cross-links introduced into the polyplex micelle core contribute to the stabilization of its structure in the extracellular entity while facilitating smooth release of the entrapped pDNA, in response to the reductive environment, inside the cells.[10,11] The outer hydrophilic shell layer, formed by PEG segment, increases complex stability in serum, avoiding nonspecific interactions with plasma proteins and reduces polymer toxicity.[12]

In this study, cross-linked polyplex micelles were systemically administered to mice bearing subcutaneously xenografted BxPC3 human pancreatic adenocarcinoma and evaluated for their transfection efficiency. Note that BxPC3 xenografts, as some intractable solid tumors, are characterized by stroma-rich histology,[13] which limits access of therapeutic agents to tumor cells. Thus, the accessibility of endothelial cells by bloodstream makes an antiangiogenic approach an attractive strategy against this model. Here we report a potent tumor growth inhibitory effect achieved by effective antiangiogenic ability by the polyplex micelles with an optimal cross-linking degree, which enables the selective expression of loaded sFlt-1 gene in tumor tissue.

Experimental Section

Materials. pDNA for luciferase (Luc) with the pCAcc vector having the CAG promoter was provided by RIKEN Gene Bank (Tsukuba, Japan) and amplified in competent DH5α *Escherichia coli*, followed by purification using a NucleoBond Xtra Maxi (Machery-Nagel GmbH & Co. KG, Düren, Germany). Dulbecco's modified Eagle's medium (DMEM) and RPMI 1640 medium were purchased from Sigma-Aldrich Co. (Madison, WI). Fetal bovine serum (FBS) was purchased from Dainippon Sumitomo Pharma Co., Ltd. (Osaka, Japan). Alexa488- and Alexa647-conjugated secondary antibodies to rat IgG were obtained from Invitrogen Molecular Probes (Eugene, OR). Human soluble VEGF R1/

(1) Folkman, J. Tumor Angiogenesis: Therapeutic Implications. *N. Engl. J. Med.* **1971**, *285*, 1182–1186.
(2) Quesada, A. R.; Munoz-Chapuli, R.; Medina, M. A. Anti-angiogenic Drugs: from Bench to Clinical Trials. *Med. Res. Rev.* **2006**, *26*, 483–530.
(3) Shibuya, M.; Yamaguchi, S.; Yamane, A.; Ikeda, T.; Tojo, A.; Matsushime, H.; Sato, M. Nucleotide Sequence and Expression of a Novel Human Receptor-type Tyrosine Kinase Gene (flt) Closely Related to the Fms Family. *Oncogene* **1990**, *5*, 519–524.
(4) Kendall, R. L.; Thomas, K. A. Inhibition of Vascular Endothelial Cell Growth Factor Activity by an Endogenously Encoded Soluble Receptor. *Proc. Natl. Acad. Sci. U.S.A.* **1993**, *90*, 10705–10709.
(5) Kendall, R. L.; Wang, G.; Thomas, K. A. Identification of a Natural Soluble Forma of the Vascular Endothelial Growth Factor Receptor, FLT-1, and Its Heterodimerization with KDR. *Biochem. Biophys. Res. Commun.* **1996**, *226*, 324–428.
(6) Kong, H. L.; Hecht, D.; Song, W.; Kovesdi, I.; Hackett, N. R.; Yayon, A.; Crystal, R. G. Regional Suppression of Tumor Growth by In Vivo Transfer of a cDNA Encoding a Secreted form of the Extracellular Domain of the Flt-1 Vascular Endothelial Growth Factor Receptor. *Hum. Gene Ther.* **1998**, *9*, 823–833.
(7) Kuo, C. J.; Farnebo, F.; Yu, E. Y.; Christofferson, R.; Swearingen, R. A.; Charter, R.; von Recum, H. A.; Yuan, J.; Kamihara, J.; Flynn, E.; D' Amato, R.; Folkman, J.; Mulligan, R. C. Comparative Evaluation of the Antitumor Activity of Antiangiogenic Proteins Delivered by Gene Transfer. *Proc. Natl. Acad. Sci. U.S.A.* **2001**, *98*, 4605–4610.
(8) Kim, W. J.; Yockman, J. W.; Jeong, J. H.; Christensen, L. V.; Lee, M.; Kim, Y. H.; Kim, S. W. Anti-angiogenic Inhibition of Tumor Growth by Systemic Delivery of PEI-g-PEG-RGD/pCMV-sFlt-1 Complexes in Tumor-bearing Mice. *J. Controlled Release* **2006**, *114*, 381–388.
(9) Kommareddy, S.; Amiji, M. Antiangiogenic Gene Therapy with Systemically Administered sFlt-1 Plasmid DNA in Engineered Gelatin-based Nanovactors. *Cancer Gene Ther.* **2007**, *14*, 488–498.
(10) Miyata, K.; Kakizawa, Y.; Nishiyama, N.; Harada, A.; Yamasaki, Y.; Koyama, H.; Kataoka, K. Block Catiomer Polyplexes with Regulated Densities of Charge and Disulfide Cross-linking Directed to Enhance Gene Expression. *J. Am. Chem. Soc.* **2004**, *126*, 2355–2361.
(11) Miyata, K.; Kakizawa, Y.; Nishiyama, N.; Yamasaki, Y.; Watanabe, T.; Kohara, M.; Kataoka, K. Freeze-dried Formulations for *In Vivo* Gene Delivery of PEGylated Polyplex Micelles with Disulfide Crosslinked Cores to the Liver. *J. Controlled Release* **2005**, *109*, 15–23.
(12) Itaka, K.; Yamauchi, K.; Harada, A.; Nakamura, K.; Kawaguchi, H.; Kataoka, K. Polyion Complex Micelles from Plasmid DNA and Poly(ethylene glycol)-poly(L-lysine) Block Copolymer as Serum-tolerable Polyplex System: Physicochemical Properties of Micelles Relevant to Gene Transfection Efficiency. *Biomaterials* **2003**, *24*, 4495–4506.
(13) Kano, M. R.; Bae, Y.; Iwata, K.; Morishita, Y.; Yashiro, M.; Oka, M.; Fujii, T.; Komuro, A.; Kiyono, K.; Kaminishi, M.; Hirakawa, K.; Ouchi, Y.; Nishiyama, N.; Kataoka, K.; Miyazono, K. Improvement of Cancer-targeting Therapy, Using Nanocarriers for Intractable Solid Tumors by Inhibition of TGF-beta Signaling. *Proc. Natl. Acad. Sci. U.S.A.* **2007**, *104*, 3460–3465.

Flt-1 immunoassay kit was purchased from R&D Systems, Inc. (Minneapolis, MN). Gemcitabine was obtained from Eli Lilly and Company (Indianapolis, IN). Avastin was obtained from F. Hoffmann-La Roche, Ltd. (Basel, Switzerland). Synthesis of thiolated block copolymer, and construction and confirmation of pDNA encoding sFlt-1 are shown in the Supporting Information. A block copolymer with *X*% of thiolation degree was abbreviated as "B-SH*X*%".

Cell Lines and Animals. Human embryonic kidney 293T cells (from RIKEN CELL BANK, Tsukuba, Japan) and human pancreatic adenocarcinoma BxPC3 cells (from ATCC, Manassas, VA) were maintained in DMEM and RPMI medium, respectively, supplemented with 10% FBS in a humidified atmosphere containing 5% CO_2 at 37 °C. 293T cells were chosen for *in vitro* experiments as cells that did not express sFlt-1.[14] Balb/c nude mice (female, 5 weeks old) were purchased from Charles River Laboratories (Tokyo, Japan). All animal experimental protocols were performed in accordance with the Guide for the Care and Use of Laboratory Animals as stated by the National Institutes of Health.

Preparation of Polyplex Micelles. Each block copolymer was dissolved in 10 mM Tris-HCl buffer (pH 7.4), followed by the addition of 10-times-excess mol of dithiothreitol (DTT) against thiol groups. After 30 min incubation at room temperature, the polymer solution was added to a twice-excess volume of 225 μg/mL pDNA/10 mM Tris-HCl (pH 7.4) solution to form polyplex micelles with N/P ratio = 2. Note that N/P ratio was defined as the residual molar ratio of amino groups of thiolated PEG-PLys to phosphate groups of pDNA. The final pDNA concentration was adjusted to 150 μg/mL. After overnight incubation at room temperature, the polyplex micelle solution was dialyzed against 10 mM Tris-HCl buffer (pH 7.4) containing 0.5 vol% DMSO at 37 °C for 24 h to remove the impurities, followed by 24 h of additional dialysis against 10 mM Tris-HCl buffer (pH 7.4) or 10 mM Hepes buffer (pH 7.4) to remove DMSO. During the dialysis, the thiol groups of thiolated block copolymers were oxidized to form disulfide cross-links. In the *in vivo* experiments, the polyplex micelle solution was adjusted to a concentration of 100 μg of pDNA/mL in 10 mM Hepes buffer (pH 7.4) with 150 mM NaCl.

Dynamic Light Scattering (DLS) Measurement. The size of the polyplex micelles was evaluated by DLS using Nano ZS (ZEN3600, Malvern Instruments, Ltd., U.K.). A He−Ne ion laser (633 nm) was used as the incident beam. Polyplex micelle solutions with N/P = 2 from 3 different batches were adjusted to a concentration of 33.3 μg of pDNA/mL in 10 mM Tris-HCl buffer (pH 7.4). The data obtained at a detection angle of 173° and a temperature of 37 °C were analyzed by a cumulant method to obtain the hydrodynamic diameters and polydispersity indices (μ/Γ^2) of micelles.

Zeta-Potential Measurement. The zeta-potential of polyplex micelles was evaluated by the laser-Doppler electrophoresis method using Nano ZS with a He−Ne ion laser (633 nm). Polyplex micelle solutions with N/P = 2 from 3 different batches were adjusted to a concentration of 33.3 μg pDNA/mL in 10 mM Tris-HCl buffer (pH 7.4). The zeta-potential measurements were carried out at 37 °C. A scattering angle of 173 °C was used in these measurements.

Real-Time Gene Expression. 293T cells (100,000 cells) were seeded on a 35 mm dish and incubated overnight. After replacement with fresh medium containing 0.1 mM D-luciferin, each type of polyplex micelle (N/P = 2) containing 3 μg of Luc pDNA was added. The dishes were set in a luminometer incorporated in a CO_2 incubator (AB-2550 Kronos Dio, ATTO, Tokyo, Japan), and the bioluminescence was monitored every 10 min with an exposure time of 1 min. Reproducibility was confirmed by triplicate experiments.

Antitumor Activity Assay. Balb/c nude mice were inoculated subcutaneously with BxPC3 cells (5×10^6 cells in 100 μL of PBS). Tumors were allowed to grow for 2−3 weeks to reach the proliferative phase (the size of the tumors at this point was approximately 60 mm^3). Subsequently, polyplex micelles (20 μg of pDNA/mouse), gemcitabine (100 mg/kg), or Avastin (50 mg/kg) maintained in 10 mM Hepes buffer (pH 7.4) with 150 mM NaCl were injected via the tail vein either 3 times (Figure 2a) or 5 times (Figure 2b) at 4-day intervals. Gemcitabine and Avastin doses and injection regimens were according to the previous reports published elsewhere.[15,16] A polyplex micelle containing Luc pDNA was used as a control formulation containing the nontherapeutic gene. Tumor size was measured every second day by a digital vernier caliper across its longest (a) and shortest diameters (b), and its volume (V) was calculated according to the formula $V = 0.5ab^2$.

***In Vivo* sFlt-1 Gene Expression.** Polyplex micelles loading either sFlt-1 or Luc pDNA (20 μg pDNA) were injected into the BxPC3-inoculated mice via the tail vein on days 0 and 4. Mice were sacrificed on day 6 after collecting blood, and the lungs, livers, spleens, kidneys, and tumors were excised. The excised organs were treated in 500 μL of cell culture lysis buffer (Promega, Madison, WI), homogenized, and centrifuged. The sFlt-1 concentration of supernatants was evaluated using the immunoassay kit according to the manufacturer's protocol. Note that block copolymers and polyplex micelles did not interfere with ELISA (Figure 2 in the Supporting Information).

Vascular Density in the Tumors. Polyplex micelles loading either sFlt-1 or Luc pDNA (20 μg of pDNA) and Avastin (50 mg/kg) were injected into the BxPC3-inoculated

(14) Kim, W. J.; Yockman, J. W.; Lee, M.; Jeong, J. H.; Kim, Y. H.; Kim, S. W. Soluble Flt-1 Gene Delivery Using PEI-g-PEG-RGD Conjugate for Anti-angiogenesis. *J. Controlled Release* **2005**, *106*, 224–234.

(15) Braakhuis, B. J. M.; van Dongen, G. A. M. S.; Vermorken, J. B.; Snow, G. B. Preclinical In Vivo Activity 2′,2′-Difluorodeoxycytidine (Gemcitabine) against Human Head and Neck Cancer. *Cancer Res.* **1991**, *51*, 211–214.

(16) Gerber, H. P.; Ferrara, N. Pharmacology and Pharmacodynamics of Bevacizumab as Monotherapy or in Combination with Cytotoxic Therapy in Preclinical Studies. *Cancer Res.* **2005**, *65*, 671–680.

mice via the tail vein on days 0 and 4. Mice were sacrificed on day 6, and the tumors were excised, frozen in dry-iced acetone, and sectioned at 10 μm thickness in a cryostat. Vascular endothelial cells (VECs) were immunostained by rat monoclonal antibody antiplatelet endothelial cell adhesion molecule-1 (PECAM-1) (BD Pharmingen, Franklin Lakes, NJ) and Alexa488-conjugated secondary antibody. The samples were observed with a confocal laser scanning microscope (CLSM). The CLSM observation was performed using an LSM 510 (Carl Zeiss, Oberlochen, Germany) with an EC Plan-Neoflur 20× objective (Carl Zeiss) at the excitation wavelength of 488 nm (Ar laser). The PECAM-1-positive area (%) was calculated from Alexa488-positive pixels.

***In Vivo* EGFP Gene Expression in the Tumors.** Polyplex micelles loading EGFP pDNA (20 μg of pDNA) were injected into the BxPC3-inoculated mice via the tail vein. Mice were sacrificed on either day 3 or day 7. Tumors were excised, fixed with 10% formalin, frozen, and sectioned. VECs were immunostained by anti-PECAM-1 antibody and Alexa647-conjugated secondary antibody. After nuclear staining with Hoechst 33342, CLSM observation was carried out using the LSM 510 with the EC Plan-Neoflur 20× objective at the excitation wavelength of 488 nm for EGFP expression, 633 nm (He−Ne laser) for Alexa647, and 710 nm (MaiTai laser, two photon excitation; Spectra-Physics, Mountain View, CA) for Hoechst 33342, respectively. The representative images of tumors excised on day 3 are shown in Figure 5. Note that images of tumors excised on day 7 showed similar patterns to those on day 3, however with lower intensity of EGFP expression.

Results

Formation of Polyplex Micelles. No free pDNA was detected by agarose gel electrophoresis, confirming that all pDNA was entrapped in disulfide cross-linked polyplex micelles, which were prepared as previously reported through ion complexation of block copolymers with pDNA at the N/P ratio = 2. Free thiol groups in polyplex micelles were estimated to be less than 2% by Ellman's test (data not shown), which is consistent with our previous report.[10] Weight−weight % ratios of pDNA/micelle in each formulation were as follows: 32.8% in B-SH0% formulation; 31.0% in B-SH5%; 29.2% in B-SH11%; 26.4% in B-SH20%; and 21.0% in B-SH36%. The mean size of the micelles was between 100 and 150 nm, with a moderate polydispersity index between 0.17 and 0.2 (Figure 3 in the Supporting Information), while zeta-potential revealed approximately neutral values, confirming the formation of PEG palisade surrounding the polyplex core (Table 1).

Real-Time Gene Expression. *In vitro* real-time Luc gene expression of polyplex micelles was evaluated using Kronos

Table 1. Sizes and Zeta-Potentials of Polyplex Micelles with Various Cross-Linking Rates at N/P = 2[a]

thiolation degree (%)	cumulant diameter (nm)	polydispersity index (μ/I^{-2})	zeta-potential (mV)
0	107 ± 2	0.195 ± 0.021	1.66 ± 0.28
5	117 ± 2	0.184 ± 0.011	1.25 ± 0.40
11	116 ± 2	0.171 ± 0.013	1.02 ± 0.30
20	139 ± 6	0.182 ± 0.050	0.40 ± 0.07
36	147 ± 2	0.192 ± 0.061	−0.96 ± 0.02

[a] The results reported were expressed as mean ± SEM (n = 3).

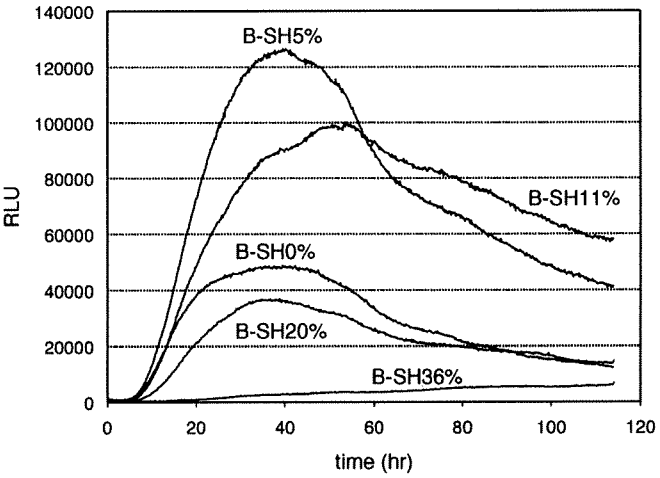

Figure 1. Real-time luciferase gene expression of the polyplex micelles with varying thiolation degrees at N/P = 2 against 293T cells.

Dio for a prolonged period (Figure 1).[17,18] The B-SH5% cross-linked polyplex micelle showed the highest gene expression among all micelles until 60 h. Worth mentioning is that the transfection efficiency of the B-SH11% micelle continued to exceed that of the B-SH5% micelle after 60 h. Disulfide cross-links in the polyplex core are believed to contribute not only to enhanced stability of the micelles in the medium but also to sustained release of complexed pDNA inside the cells with a reductive environment, resulting in polyplex micelles with higher cross-linking rates that can maintain an appreciable transfection efficiency over a longer time scale. Note that the B-SH36% micelle showed an increasing trend in gene expression with time.

Antitumor Activity. Polyplex micelles containing sFlt-1 pDNA were injected iv into mice bearing pancreatic adenocarcinoma BxPC3, followed by evaluation of tumor volume (Figure 2). All the micelles were injected three times on days

(17) Takae, S.; Miyata, K.; Oba, M.; Ishii, T.; Nishiyama, N.; Itaka, K.; Yamasaki, Y.; Koyama, H.; Kataoka, K. PEG-detachable Polyplex Micelles Based on Disulfide-crosslinked Block Catiomers as Bioresponsive Nonviral Gene Vectors. *J. Am. Chem. Soc.* **2008**, *130*, 6001–6009.

(18) Oba, M.; Aoyagi, K.; Miyata, K.; Matsumoto, Y.; Itaka, K.; Nishiyama, N.; Yamasaki, Y.; Koyama, H.; Kataoka, K. Polyplex Micelles with Cyclic RGD Peptide Ligands and Disulfide Cross-links Directing to the Enhanced Transfection via Controlled Intracellular Trafficking. *Mol. Pharmaceutics* **2008**, *5*, 1080–1092.

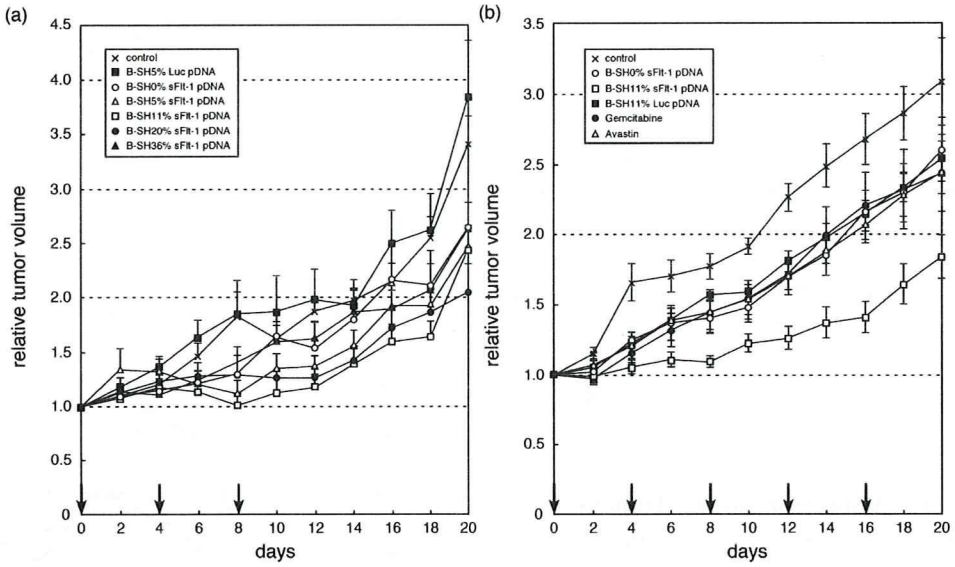

Figure 2. Antitumor activity of polyplex micelles with sFlt-1 pDNA in subcutaneously BxPC3-inoculated mice. (a) Effect of thiolation degree. Hepes buffer (control) was used as a negative control. Polyplex micelles were injected iv on days 0, 4, and 8 at 20 μg pDNA/mouse, and mice were monitored for the relative tumor volume every second day. Error bars represent the SEM ($n = 6$). Only the B-SH11% polyplex micelles exhibited significant retardation of tumor growth compared to the control ($P < 0.01$). (b) Growth curve study with an increased dose of the B-SH11% polyplex micelles compared to commercially available drugs. Polyplex micelles (20 μg pDNA/mouse), gemcitabine (100 mg/kg), and Avastin (50 mg/kg) were injected iv on days 0, 4, 8, 12, and 16. Relative tumor size was measured every second day. Hepes buffer (control) was used as a negative control. Error bars represent the SEM ($n = 5$). Only the B-SH11% polyplex micelles exhibited significant retardation of tumor growth compared to the control ($P < 0.001$). P values were calculated by multivariate ANOVA study.

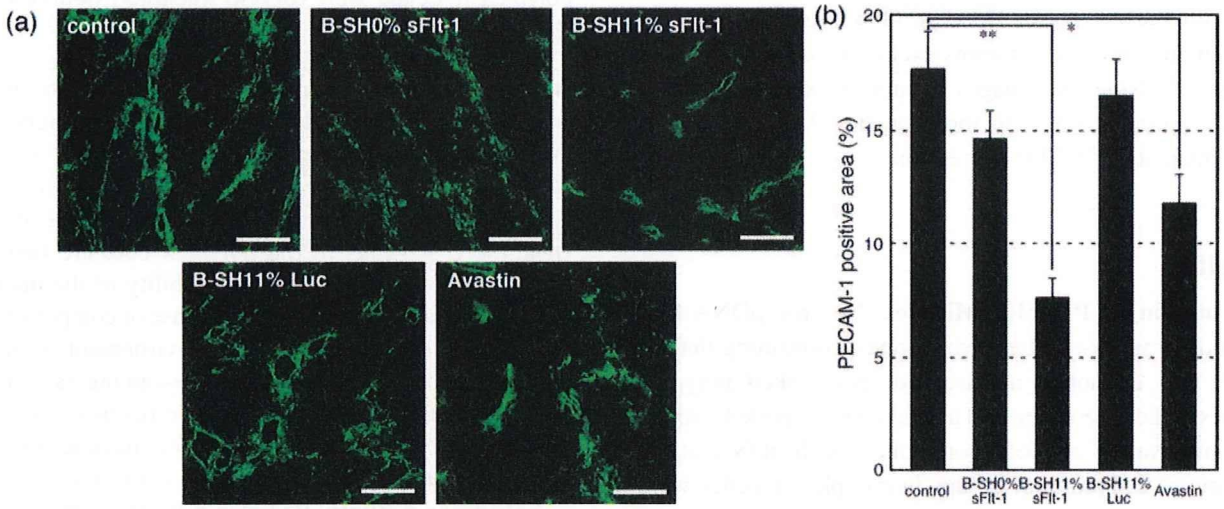

Figure 3. Immunostaining of the VECs in the BxPC3 tumor tissue by PECAM-1 antibody. Hepes buffer (control), three types of polyplex micelles (20 μg of pDNA/mouse), and Avastin (50 mg/kg) were injected into the BxPC3-inoculated mice via the tail vein on days 0 and 4. Mice were sacrificed on day 6, and tumors were excised and immunostained. (a) CLSM images of immunostained tumors. PECAM-1-positive regions are green. Bars represent 100 μm. (b) Areas of PECM-1-positive endothelium were quantified. Error bars represent the SEM ($n = 15$). P values were calculated by Student's t test. $^*P < 0.01$ and $^{**}P < 0.001$.

0, 4, and 8 (Figure 2a). The B-SH11% micelle significantly suppressed tumor growth compared to control mice treated with Hepes buffer ($P < 0.01$). There was no significant change in tumor growth after injection of other polyplex micelles, implying that an optimal cross-linking rate is required to achieve an effective expression of the gene. Encouraged by these results, the tumor growth suppression activity of B-SH11% micelle was further evaluated, implying a regimen with enhanced number of injections. The effect of the micelles was compared to commercially available drugs, gemcitabine, a standard chemotherapeutic agent for pancreatic tumor, and bevacizumab (Avastin), a monoclonal antibody against VEGF (Figure 2b). The doses of gemcitabine and Avastin implied in our study were based on

previous reports published elsewhere.[15,16] The administration of B-SH11%/sFlt-1 micelle resulted in significant suppression of tumor growth ($P < 0.001$), while gemcitabine and Avastin, under the reported experimental regimen, showed no remarkable therapeutic effect. Note that the difference observed in tumor volumes between the B-SH11%/Luc micelle-treated group and the control group was not significant.

Tumor Vascular Density. The antiangiogenic effect of expressed sFlt-1 was confirmed by immunostaining of VECs using PECAM-1 (Figure 3). Vascular density of tumors treated with either B-SH11%/sFlt-1 micelle or Avastin was significantly lower than that of the other groups. The most pronounced and significant effect on neo-vasculature suppression was achieved by B-SH11%/sFlt-1 micelle (7% PECAM-1 positive area) over Avastin (12% PECAM-1 positive area) ($P < 0.05$). These results suggest that the expressed sFlt-1 may entrap VEGF secreted in the tumor tissue, thereby suppressing the growth of VECs.

***In Vivo* sFlt-1 Gene Expression.** Expression levels of sFlt-1 in the body were then evaluated by measuring the amount of sFlt-1 in lung, liver, spleen, kidney, tumor, and blood plasma using enzyme-linked immunosorbent assay (ELISA) (Figure 4). Injection of B-SH11%/sFlt-1 micelle resulted in significantly higher expression of sFlt-1 selectively in tumor tissue compared to the control. On the other hand, injection of B-SH0%/sFlt-1 micelle or B-SH11%/Luc micelle did not result in any difference in sFlt-1 expression compared to the control. These results strongly support that tumor-specific elevation in sFlt-1 expression led to the significant growth suppression of VECs in the tumor tissue and, eventually, the suppression of tumor growth.

***In Vivo* Enhanced Green Fluorescence Protein (EGFP) Gene Expression in Tumors.** The location of gene expression in BxPC3 tumors after administration of the micelles was analyzed histologically using pDNA encoding EGFP (Figure 5). As previously reported,[13,19,20] thick fibrotic tissue was formed around blood vessels (red) inside the stroma of BxPC3 tumors, and nests of tumor cells (region T) were scattered in the stroma (Figure 5a). The expression of EGFP (Figures 5b and 5c) was observed mainly in the VECs and cells in stromal regions adjacent to some vasculature, indicating that VECs and fibroblasts near some vasculature in the stroma, but not the tumor cells, were transfected. As seen in Figure 5a, there were thick fibrotic tissues around blood vessels in the BxPC3 xenograft,

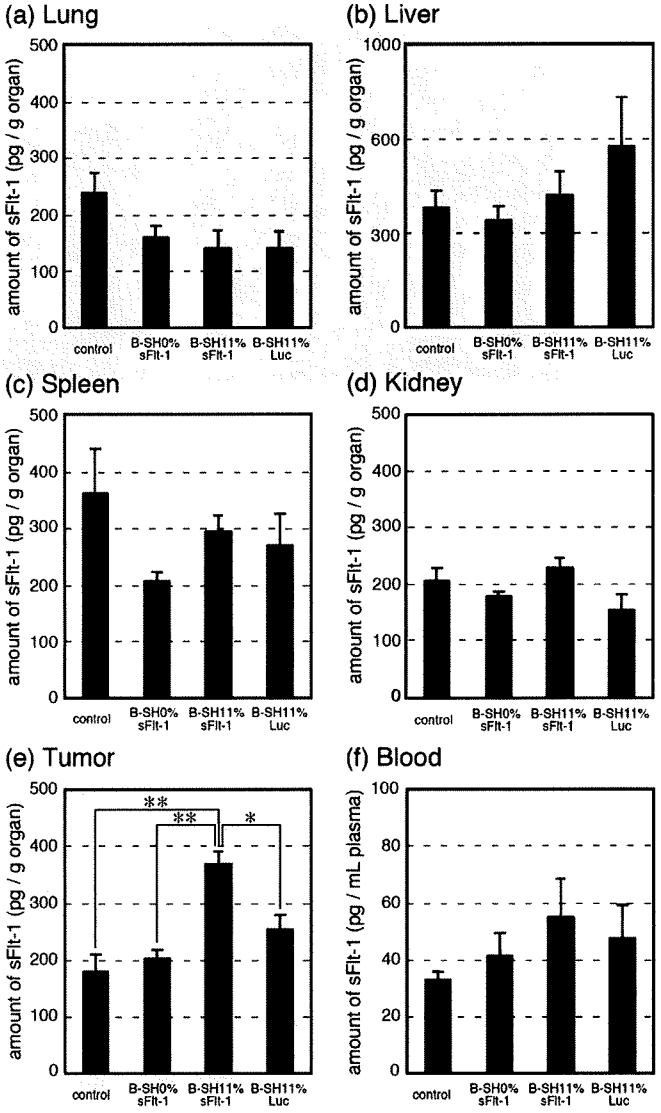

Figure 4. Evaluation of sFlt-1 gene expression in organs by ELISA. Hepes buffer (control) and three types of polyplex micelles (20 μg pDNA/mouse) were injected into the BxPC3-inoculated mice via the tail vein on days 0 and 4. Mice were sacrificed on day 6 after collecting blood (f), and the lungs (a), livers (b), spleens (c), kidneys (d), and tumors (e) were excised, followed by evaluation of sFlt-1 concentration by ELISA according to the manufacturer's protocol. Error bars represent the SEM ($n = 6$). P values were calculated by Student's t test. $^*P < 0.01$ and $^{**}P < 0.001$.

indicating that the penetration of polyplex micelles deep into the stroma or into the tumor nest was interrupted and the gene expression was limited in the VECs and some of the fibroblasts in the stroma. Higher levels of EGFP expression were observed for B-SH11% micelle, confirming their enhanced ability to accumulate inside tumor tissue compared to B-SH0% micelle.

Discussion

Since all solid tumors need angiogenesis for their growth, antiangiogenic therapy is a promising strategy for treating

(19) Miyata, K.; Oba, M.; Kano, M. R.; Fukushima, S.; Vachutinsky, Y.; Han, M.; Koyama, H.; Miyazono, K.; Nishiyama, N.; Kataoka, K. Polyplex Micelles from Triblock Copolymers Composed of Tandemly Aligned Segments with Biocompatible, Endosomal Escaping, and DNA-condensing Functions for Systemic Gene Delivery to Pancreatic Tumor Tissue. *Pharm. Res.* **2008**, *25*, 2924–2936.

(20) Kano, M. R.; Komuta, Y.; Iwata, K.; Oka, M.; Shirai, Y.; Morishita, Y.; Ouchi, Y.; Kataoka, K.; Miyazono, K. Comparison of the Effects of the Kinase Inhibitors Imatinib, Sorafenib, and Transforming Growth Factor-β Receptor Inhibitor on Extravasation of Nanoparticles from Neovasculature. *Cancer Sci.* **2009**, *100*, 173–180.

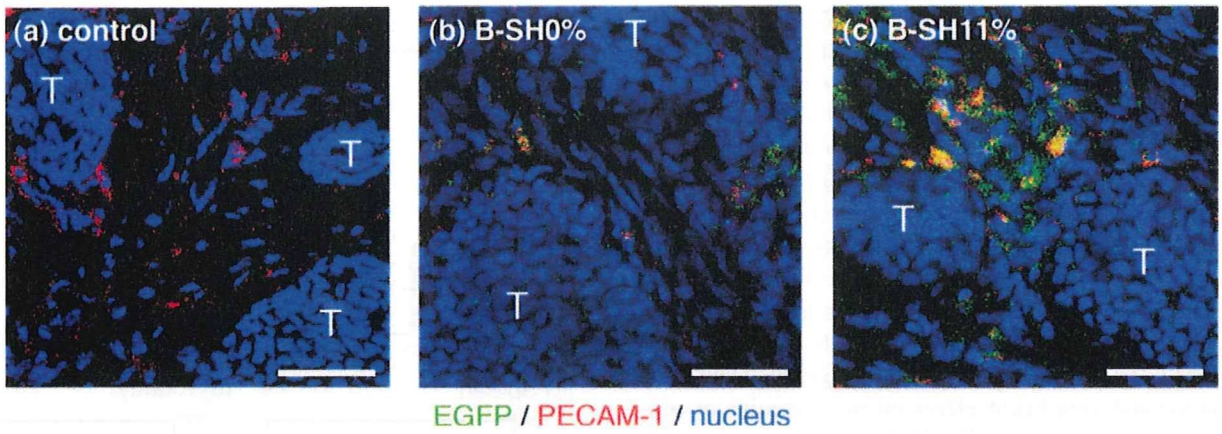

Figure 5. EGFP gene expression by polyplex micelles in the inoculated BxPC3 tumors. Hepes buffer (a) was used as a negative control. B-SH0% (b) and B-SH11% (c) polyplex micelles containing EGFP pDNA (20 μg pDNA/mouse) were injected into the BxPC3-inoculated mice via the tail vein. Mice were sacrificed on day 3, and tumors were excised and immunostained. "T" indicates nests of tumor cells in tumor tissues. Bars represent 50 μm.

tumor patients. In fact, Avastin, the recombinant humanized monoclonal antibody against VEGF, has been widely used as an antiangiogenic drug, and its application range is spreading to the various types of solid tumors.[16] Other antiangiogenic proteins,[21,22] e.g., angiostatin, endostatin, and soluble forms of VEGF receptor, have also received great attention. Meanwhile, antiangiogenic gene therapy represents an attractive alternative to antiangiogenic proteins for reasons such as low dose, continuous expression of the therapeutic protein, and low cost. Therefore, development of an effective and safe gene vector is a key to successful antiangiogenic gene therapy.

In this study, thiolated PEG-PLys block copolymers were applied in the formation of disulfide cross-linked polyplex micelles for delivery of pDNA encoding sFlt-1, and tested for their antiangiogenic effect on mice bearing xenografted BxPC3 cell line, derived from human pancreatic adenocarcinoma. Disulfide cross-links in the polyplex core were designed to increase blood stability of the polyplex micelles and effectively release pDNA in the intracellular milieu.[10,11,18] PEG palisade of the polyplex micelle is expected to cover the polyplex core to shield the positive charge as well as to decrease interfacial free energy.[12,23] The formation of the PEG palisade surrounding the polyplex core was confirmed by the neutral zeta-potential of the polyplex micelles (Table 1). B-SH36% micelle showed an approximately 10 times higher concentration of pDNA in the blood at 60 min after iv injection than that of the micelle without core cross-linking (B-SH0%) (Figure 4 in the Supporting Information). The disulfide cross-links in the polyplex core apparently contribute to the enhanced stability of the micelles in the bloodstream. Note that the size of polyplex micelles is between 100 and 150 nm (Table 1), which may be in a suitable range for accumulation in solid tumors due to the enhanced permeability and retention (EPR) effect,[24] although the size may be too large to allow the micelles to penetrate into the stroma in pancreatic tumors.[13] Nevertheless, there is a concern that excessive disulfide cross-links interfere with the smooth release of entrapped pDNA in the core, resulting in decreased transfection efficiency.[10] Accordingly, optimal cross-linking density should be determined to balance the stability and maintain high transfection efficiency. The results of *in vitro* real-time gene expression showed that B-SH5% micelle possessed the highest efficiency among the evaluated samples up to 60 h after transfection. It is noteworthy that B-SH11% micelle exerted sustained Luc expression and kept an appreciably high efficiency beyond 60 h (Figure 1). Apparently, gene expression is prolonged with an increase in cross-linking rates, although excess cross-links induced overstabilization of polyplex micelles, resulting in decreased transfection efficiency in the case of the B-SH20% and B-SH36% micelles. Eventually, the B-SH36%/sFlt-1 micelle had no *in vivo* efficiency, even though they showed the highest stability in the bloodstream among the evaluated samples (Figure 4 in the Supporting Information). It is also noteworthy that the B-SH11%/sFlt-1 micelle achieved an appreciably high therapeutic efficiency, even though it showed only limited improvement in blood circulation time compared to the B-SH0% and B-SH5% systems. Presumably, a sustained

(21) Sim, B. K. L.; MacDonald, N. J.; Gubish, E. R. Angiostatin and Endostatin: Endogenous Inhibitors of Tumor Growth. *Cancer Metastasis Rev.* **2000**, *19*, 181–190.

(22) Fischer, C.; Mazzone, M.; Jonckx, B.; Carmeliet, P. FLT1 and Its Ligands VEGFB and PIGF: Drug Targets for Anti-angiogenic Therapy. *Nat. Rev. Cancer* **2008**, *8*, 942–956.

(23) Kakizawa, Y.; Kataoka, K. Block Copolymer Micelles for Delivery of Gene and Related Compounds. *Adv. Drug Delivery Rev.* **2002**, *54*, 203–222.

(24) Matsumura, Y.; Maeda, H. A New Concept for Macromolecular Therapeutics in Cancer Chemotherapy: Mechanism of Tumoritropic Accumulation of Proteins and the Antitumor Agent Smancs. *Cancer Res.* **1986**, *46*, 6387–6392.

profile in gene expression may have been the key to this achievement. Note that no change in body weight of the mice was observed during the experiment (data not shown), indicating few serious side effects of polyplex micelles.

Comparison with the commercially available agents, gemcitabine and Avastin, confirmed the encouraging tumor growth suppression effect of the B-SH11% polyplex micelle (Figure 2b). Gemcitabine continues to be the standard therapy in the treatment of pancreatic tumors; however, its objective response rate is limited in patients with advanced disease.[25] Avastin is a recombinant humanized monoclonal antibody against human VEGF, which may neutralize tumor-cell-derived VEGF in the model used here. In humans, Avastin is the first clinically available antiangiogenic drug, and it has been efficient when used in combined chemotherapy for metastatic colorectal cancer[26] and non-small-cell lung cancer.[27] However, it showed no benefit in patients with pancreatic tumors.[25] The B-SH11%/sFlt-1 micelle significantly suppressed tumor growth compared not only to the control ($P < 0.001$) but also to the B-SH11%/Luc micelle, gemcitabine, and Avastin ($P < 0.01$) (Figure 2b). Xenografted BxPC3 was reported not to respond to gemcitabine,[28] probably due to its inability to penetrate through the tumor thick fibrotic tissue and target tumor cells, which is consistent with our results. Evaluation of vascular density in BxPC3 tumor (Figure 3) clearly showed that the B-SH11%/sFlt-1 micelle decreased vascular density compared to the control ($P < 0.001$), the B-SH11%/Luc micelle ($P < 0.001$), and Avastin ($P < 0.05$) treated tumors.

Inhibitory effect on tumor growth (Figure 2) is consistent with the result of decreased vascular density. There are several studies on antiangiogenic gene therapy for subcutaneously inoculated tumors in mice by systemic expression of sFlt-1 using viral vectors, including im injection of adeno-associated viral vectors[29] and iv injection of adenoviral vectors to target livers.[30] In these studies, however, sFlt-1 was expressed mainly in organs rather than tumor tissue. What was worse, the excess expression of sFlt-1 in the liver led to unacceptable hepatotoxicity.[31] Thus, tumor-specific expression of sFlt-1 is essential for a safe and efficient antiangiogenic gene therapy. However, any nonviral gene vectors loading sFlt-1 gene have failed to exhibit selective gene expression in the tumor tissue, although they achieved certain inhibition of tumor growth.[8,9] In this regard, the B-SH11%/sFlt-1 micelle system might be promising, since sFlt-1 expression was significantly increased selectively in the tumor tissue compared not only to the control ($P < 0.001$) but also to the B-SH11%/Luc micelle ($P < 0.01$), as shown in Figure 4, without any significantly enhanced expression in other normal tissues. Note that no significant increase of sFlt-1 expression was observed in any normal organs treated with B-SH0%/sFlt-1 micelle or B-SH11%/Luc micelle. Histological analyses revealed that EGFP expression of the B-SH11%/EGFP micelle was located mainly around VECs but not in the tumor cells (Figure 5), probably due to restricted permeation of micelles by thick fibrotic tissues and pericyte-covered vasculature of the BxPC3 tumors. These results suggested the ability of expressed sFlt-1 molecule to entrap excess VEGF in the tumor tissue and to inhibit tumor growth by an antiangiogenic effect. Xenografted BxPC3 tumors in mice are characterized by stroma-rich histology,[20] which might explain the only slight inhibitory effects on BxPC3 growth achieved by gemecitabine[28] targeting tumor cells.

Conclusions

In conclusion, antiangiogenic gene therapeutic study was carried out by iv administration of polyplex micelles with sFlt-1 pDNA to mice bearing pancreatic adenocarcinoma BxPC3 xenografts, and the results demonstrated the ability of B-SH11% sFlt-1 micelle as a safe and effective gene delivery system. The optimal disulfide cross-linking rate of polyplex micelles was found to show significant suppression of tumor growth. Gene expression of sFlt-1 by iv injection of polyplex micelles was observed in tumor tissue only, followed by decreased vascular density and significant suppression of tumor growth. Based on these results, the B-SH11% disulfide cross-linked polyplex

(25) Rocha-Lima, C. M. New Directions in the Management of Advanced Pancreatic Cancer: a Review. *Anti-Cancer Drugs* **2008**, *19*, 435–446.

(26) Hurwitz, H.; Fehrenbacher, L.; Novotny, W.; Cartwright, T.; Hainsworth, J.; Heim, W.; Berlin, J.; Baron, A.; Griffing, S.; Holmgren, E.; Ferrara, N.; Fyfe, G.; Rogers, B.; Ross, R.; Kabbinavar, F. Bevacizumab Plus Irinotecan, Fluorouracil, and Leucovorin for Metastatic Colorectal Cancer. *N. Engl. J. Med.* **2004**, *350*, 2335–2342.

(27) Sandler, A.; Gray, R.; Perry, M. C.; Brahmer, J.; Schiller, J. H.; Dowlati, A.; Lilenbaum, R.; Johnson, D. H. Paclitaxel-carboplatin Alone or with Bevacizumab for Non-small-cell Lung Cancer. *N. Engl. J. Med.* **2006**, *355*, 2542–2550.

(28) Merriman, R. L.; Hertel, L. W.; Schultz, R. M.; Houghton, P. J.; Houghton, J. A.; Rutherford, P. G.; Tanzer, L. R.; Boder, G. B.; Grindey, G. B. Comparison of the Antitumor Activity of Gemcitabine and Ara-C in a Panel of Human Breast, Colon, Lung and Pancreatic Xenograft Models. *Invest. New Drugs* **1996**, *14*, 243–247.

(29) Takei, Y.; Mizukami, H.; Saga, Y.; Yoshimura, I.; Hasumi, Y.; Takayama, T.; Kohno, T.; Matsushita, T.; Okada, T.; Kume, A.; Suzuki, M.; Ozawa, K. Suppression of Ovarian Cancer by Muscle-Mediated Expression of Soluble VEGFR-1/Flt-1 Using Adeno-associated Virus Serotype 1-derived Vector. *Int. J. Cancer* **2006**, *120*, 278–284.

(30) Liu, J.; Li, J.; Su, C.; Huang, B.; Luo, S. Soluble Fms-like Tyrosine Kinase-1 Expression Inhibits the Growth of Multiple Myeloma in Nude Mice. *Acta Biochim. Biophys. Sin.* **2007**, *39*, 499–506.

(31) Mahasreshti, P. J.; Kataram, M.; Wang, M. H.; Stockard, C. R.; Grizzle, W. E.; Carey, D.; Siegal, G. P.; Haisma, H. J.; Alvarez, R. D.; Curiel, D. T. Intravenous Delivery of Adenovirus-mediated Soluble FLT-1 Results in Liver Toxicity. *Clin. Cancer Res.* **2003**, *9*, 2701–2710.

micelle with sFlt-1 pDNA is interesting and worthy to develop further for antiangiogenic gene therapy of solid tumors.

Acknowledgment. This work was financially supported in part by the Core Research Program for Evolutional Science and Technology (CREST) from Japan Science and Technology Agency (JST) as well as by Grants-in-Aid for Young Scientists (A) and Exploratory Research. We express our appreciation to Masabumi Shibuya (Tokyo Medical and Dental University) for providing pVL 1393 baculovirus vector pDNA encoding human sFlt-1. We thank Kazuhiro Aoyagi, Yoko Hasegawa, Kotoe Date, and Satomi Ogura (The University of Tokyo) for technical assistance.

Supporting Information Available: Synthesis of thiolated block copolymer and Supporting Figures 1, 2, 3, and 4. This material is available free of charge via the Internet at http://pubs.acs.org.

MP9002317

Journal of Controlled Release 140 (2009) 306–311

Contents lists available at ScienceDirect

Journal of Controlled Release

journal homepage: www.elsevier.com/locate/jconrel

Enhanced magnetic resonance imaging of experimental pancreatic tumor *in vivo* by block copolymer-coated magnetite nanoparticles with TGF-β inhibitor

Michiaki Kumagai [a,e,1], Mitsunobu R. Kano [b,f,1], Yasuyuki Morishita [b], Motomi Ota [a], Yutaka Imai [a], Nobuhiro Nishiyama [a,e,f], Masaki Sekino [c], Shoogo Ueno [d], Kohei Miyazono [b,f], Kazunori Kataoka [a,e,f,*]

[a] Department of Materials Engineering, Graduate School of Engineering, The University of Tokyo, 7-3-1 Hongo, Bunkyo-ku, Tokyo 113-8656, Japan
[b] Department of Molecular Pathology, Graduate School of Medicine, The University of Tokyo, 7-3-1 Hongo, Bunkyo-ku Tokyo 113-0033, Japan
[c] Department of Advanced Energy, Graduate School of Frontier Sciences, The University of Tokyo, 5-1-5, Kashiwanoha, Kashiwa-shi, Chiba, 277-8561, Japan
[d] Department of Applied Quantum Physics, Graduate School of Engineering, Kyushu University, 6-10-1 Hakozaki, Higashi-ku Fukuoka 812-8581, Japan
[e] Center for Disease Biology and Integrative Medicine, School of Medicine, The University of Tokyo, 7-3-1 Hongo, Bunkyo-ku, Tokyo 113-0033, Japan
[f] Center for NanoBio Integration, The University of Tokyo, 7-3-1 Hongo, Bunkyo-ku, Tokyo 113-8656, Japan

ARTICLE INFO

Article history:
Received 13 March 2009
Accepted 5 June 2009
Available online 12 June 2009

Keyword:
Magnetic resonance imaging
Pancreatic cancer
TGF-β
Magnetite nanoparticles
Poly(ethylene glycol)

ABSTRACT

Early detection of solid tumors, particularly pancreatic cancer, is of substantial importance in clinics. Enhanced magnetic resonance imaging (MRI) with iron oxide nanoparticles is an available way to detect the cancer. The effective and selective accumulation of these nanoparticles in the tumor tissue is needed for improved imaging, and in this regard, their longevity in the blood circulation time is crucial. We developed here block copolymer-coated magnetite nanoparticles for pancreatic cancer imaging, by means of a chelation between the carboxylic acid groups in poly(ethylene glycol)–poly(aspartic acid) block copolymer (PEG–PAsp) and Fe on the surface of the iron oxide nanoparticles. These nanoparticles had considerably narrow distribution, even upon increased ionic strength or in the presence of fetal bovine serum. The PEG–PAsp-coated nanoparticles were further shown to be potent as a contrast agent for enhanced MRI for an experimental pancreatic cancer, xenografts of the human-derived BxPC3 cell line in BALB/c nude mice, with combined administration of TGF-β inhibitor. Iron staining of tumor tissue confirmed the accumulation of the nanoparticles in tumor tissue. Use of the PEG–PAsp-coated magnetite nanoparticles, combined with the TGF-β inhibitor, is of promising clinical importance for the detection of intractable solid cancers, including pancreatic cancer.

1. Introduction

Pancreatic cancer, one of the intractable solid tumors, is the fourth leading cause of cancer-related deaths in the United States and the fifth in Japan [1]. The average survival period of patients suffering from advanced pancreatic adenocarcinoma is still extremely short, only 6 months, despite recent progress in the chemotherapies [2]. Although cancer detection and treatment have been greatly improved through the development of diagnostic imaging modalities, it is still difficult to detect pancreatic cancer [3]. Consequently, the development of diagnostic systems to detect these cancers is of great importance.

Recently, superparamagnetic iron oxide (SPIO) nanoparticles composed of either magnetite (Fe_3O_4) or maghemite (g-Fe_2O_3) have been studied as contrast agents for magnetic resonance (MR) imaging [4]. Commercial application for human diagnosis based on SPIO particles is currently available. However, since cancer detection requires the systemic administration of iron oxide nanoparticles, the circulation time of the particles must be prolonged. Several studies have already reported that the behavior of magnetic nanoparticles in the bloodstream depends closely on their nanoscale morphology, including overall diameter, size distribution, or nature of the surface [5,6]. Additionally, the surface modification of iron oxide nanoparticles has proved a versatile strategy for improving their biological performance, including the reduction of immunogenicity and enhancement of targeted delivery to specific tissues [7]. However, the overall correlation between the surface modification of nanoparticles and their *in vivo* behavior remains to be further elucidated.

Various methods of stabilization for SPIO nanoparticles have been reported to date [8]. One of the most feasible approaches could be the stabilization of SPIO by coated with biocompatible polymers [9]. Suitable polymers, including poly(ethylene glycol) (PEG) and its block copolymers, are promising for the development of SPIO systems with defined surface properties. This coating of particles with PEG, or PEGylation, to avoid their uptake by the reticuloendothelial system, is under intensive investigation. We also previously reported the accumulation of β-FeOOH nanoparticles coated with PEG–poly(α,β-aspartic acid) block copolymer

* Corresponding author. Department of Materials Engineering, Graduate School of Engineering, The University of Tokyo, 7-3-1 Hongo, Bunkyo-ku, Tokyo 113-8656, Japan.
E-mail address: kataoka@bmw.t.u-tokyo.ac.jp (K. Kataoka).
[1] Equal contribution.

0168-3659/$ – see front matter © 2009 Elsevier B.V. All rights reserved.
doi:10.1016/j.jconrel.2009.06.002

(PEG–PAsp) into experimental colon adenocarcinoma, which could be applicable for tumor-selective MR imaging [10]. The multivalent bonding of PEG-based block copolymer to magnetic nanoparticles may thus help to facilitate the accumulation of these nanoparticles into some solid tumors. However, magnetic nanoparticles of any design have not yet been successful in exhibiting sufficient accumulation in intractable solid cancers, including pancreatic adenocarcinoma [1]. In addition to improving the performance of iron-based contrast agents (e.g. biocompatibility), the co-administration of adjuvant small molecules could increase the accumulation of these agents in target cancer tissue. In fact, we have recently shown that the administration of the small molecule TGF-β inhibitor (LY364947) at a low dose [11], which could minimize the potential side effects of the TGF-β inhibitor, can alter the tumor microenvironment and enhance the EPR effect in these cancers [12]. Therefore, the combined use of TGF-β inhibitor could be promising to diagnose intractable cancers with a long-circulating MRI contrast agent. Here, we demonstrated the successful MR imaging of experimental pancreatic cancer by the systemic administration of newly developed SPIO nanoparticles coated by PEG–PAsp in aid of TGF-β inhibitor.

2. Materials and methods

2.1. Reagents

β-benzyl L-aspartate and bis(trichloromethyl)carbonate (triphosgene) were purchased from Sigma-Aldrich Corporation (St. Louis, MO, USA) and Tokyo Chemical Industry Co., Ltd. (Tokyo, Japan), respectively. α-Methoxy-ω-amino-poly(ethylene glycol) (CH_3O–PEG–NH_2; $M_w = 12\,000$) was purchased from NOF Corporation (Tokyo, Japan). Tetrahydrofuran (THF), *n*-hexane, *N*,*N*-dimethylformamide (DMF), CH_2Cl_2 were doubly-distilled according to the standard procedures. The magnetite nanoparticles were supplied by Toda Kogyo Corporation (Hiroshima, Japan; average particle size of magnetite: 10 nm). Resovist® was obtained from Bayer HealthCare Co., Ltd. (Osaka, Japan). TGF-β inhibitor was purchased from EMD Chemicals Inc. (San Diego, CA, USA) (LY364947; catalog no. 616451).

2.2. Synthesis of poly(ethylene glycol)–poly(α,β-aspartic acid) block copolymer (PEG–PAsp)

PEG–PAsp was synthesized by a previously reported procedure [13]. Briefly, poly (ethylene glycol)–*b*–poly(β-benzyl L-aspartate) block copolymer (PEG–PBLA) was prepared by ring-opening polymerization of N-carboxy anhydride of β-benzyl L-aspartate (BLA-NCA) from the ω-NH_2 group of PEG ($M_w = 1.2 \times 10^4$). Molecular weight distribution of PEG–PBLA was narrow as $M_w/M_n = 1.06$, which was determined by gel permeation chromatography [columns: TSK-gel G3000HHR, G4000HHR (Tosoh, Yamaguchi, Japan); eluent: DMF containing 10 mM LiCl; flow rate: 0.8 ml/min; detector: refractive index (RI); temperature: 40 °C]. The composition of these block copolymers was determined by ^{1}H NMR from peak intensity ratios of methylene protons of PEG (OCH_2CH_2: $d = 3.7$ ppm) and phenyl protons of the β-benzyl groups of PBLA ($-CH_2C_6H_5$: $d = 7.3$ ppm). The polymerization degree of BLA in block copolymer was calculated to be 38. The benzyl groups of PEG–PBLA were then removed by alkaline hydrolysis using 0.1 N NaOH to obtain PEG–PAsp as follows:

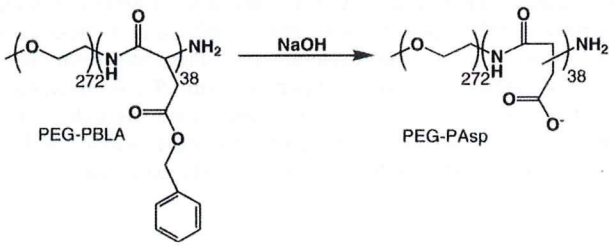

2.3. Preparation of PEG–PAsp-coated magnetite nanoparticles

PEG–PAsp-coated magnetite nanoparticles were prepared according to the previous method with slight modification [10]. Briefly, magnetite solution was quickly added to an aqueous solution of PEG–PAsp with varying feed molar ratios of aspartic acid residues to Fe ([Asp]/[Fe]) in the range of 0.01 to 1. The final concentration of magnetite was adjusted to 10 mmol/l. The mixed solutions were incubated at room temperature for 24 h to obtain magnetite nanoparticles coated with PEG–PAsp. Purification of the PEG–PAsp-coated magnetite nanoparticles was carried out by ultrafiltration (MWCO 200 000; polysulfone membrane, Toyo Roshi Co. Ltd., Tokyo, Japan).

2.4. Physicochemical characterization of the nanoparticles

The morphology and size distribution of the nanoparticles were examined by transmission electron microscopy (H-7000, Hitachi, Ltd., Tokyo, Japan) at an accelerating voltage of 75 kV. The TEM samples were prepared by mounting a drop of aqueous iron oxide nanoparticles suspension on carbon-coated 400 mesh Cu grids and allowing them to dry in air. Fourier transform infrared (FT-IR) spectra were obtained using a FT-IR spectrophotometer (FT/IR615, JASCO Corporation, Hachioji, Tokyo, Japan) with a resolution of 4 cm^{-1}. To characterize the interaction between block copolymer and magnetite nanoparticles, a small amount of nanoparticles powder was milled with KBr, and then pressed into a disc for analysis. Each spectrum was scanned 64 times to increase the signal-to-noise ratio. The Fe content in the nanoparticles was determined by ion coupled plasma-mass spectroscopy (ICP-MS, 4500, Hewlett Packard, Palo Alto, CA, USA). The amount of adsorbed block copolymer on magnetite nanoparticles was measured by thermogravimetric analysis (TGA) (EXSTAR6200 TG/DTA, Seiko Instruments Inc., Chiba, Japan) in nitrogen atmosphere with a heating rate of 10 °C/min in the temperature range of 25–1100 °C.

2.5. Light scattering and ζ-potential measurements

The size distribution of the PEG–PAsp-coated magnetite nanoparticles was examined by dynamic light scattering (DLS) DLS-7000 (Otsuka Electronics Co., Ltd., Osaka, Japan). Vertically polarized light with a wavelength of 488 nm from an Ar-ion laser (15 mW) was used as the incident beam. All measurements were conducted at 37 °C, and the data were analyzed by the cumulant method to determine the hydrodynamic diameters of the particles. The ζ-potential of PEG–PAsp-coated magnetite nanoparticles at 37 °C was measured by a Zetasizer NanoZS instrument equipped with a DTS5001 cell (Malvern Instruments Ltd., Worcestershire, UK).

2.6. Characterization of the r_2 relaxivities

The MR contrast effect of the magnetite nanoparticles was examined by measuring their proton relaxivities, r_2, of which the definition is the slope of the concentration dependence given as:

$$1/T_2 = 1/T_2(0) + r_2[\mathrm{Fe}]$$

Thus, a plot of $1/T_2$ versus concentration gives the relaxivity as the slope, where T_2 is the transversal relaxation time, $1/T_2$ is the transversal relaxation rate constant in the presence of a paramagnetic species, and $1/T_2(0)$ is the transversal relaxation rate constant in the absence of a paramagnetic species. The magnetite nanoparticles were dispersed into deionized water at concentrations of 0.5, 1.0, 1.5, 2.0, and 2.5 mM and the T_2 of these nanoparticle solutions was measured at 25 °C in water with a 0.47 T minispectrometer (Minispec, Bruker

Optics Inc., Woodlands, TX, USA) using the Carr–Purcell–Meiboom–Gill (CPMG) method [14].

2.7. In vivo MR imaging

The BxPC3 human pancreatic adenocarcinoma cell line was obtained from the American Type Culture Collection (Manassas, VA, USA). The BxPC3 cells were grown in RPMI 1640 medium supplemented with 10% FBS. BALB/c nude mice (female, 5–6 weeks of age), obtained from Charles River Laboratories Japan Inc. (Tokyo, Japan), were inoculated subcutaneously with BxPC3 cells (1×10^7 cells/mouse). After 3–4 weeks, MR imaging of the tumors was conducted with a 4.7 T scanner (INOVA200, Varian, Inc., Palo Alto, CA, USA). Twenty-four hours prior to the *in vivo* MR imaging, animals were treated with TGF-β inhibitor, 5 mg/ml in 4 μl of DMSO and diluted by 100 μl of PBS, at 1 mg/kg by intraperitoneal injection. Subsequently, the mice were injected at a dose of 0.1 mmolFe/kg, with Resovist® or PEG–PAsp-coated magnetite nanoparticles. A total of 4 conditions ($n=5$ mice each) were investigated, i.e. with or without TGF-β inhibitor for both Resovist® or PEG–PAsp-coated magnetite nanoparticles. Imaging was performed at different temporal points (e.g., preinjection, 1 h postinjection, and 2 h postinjection). For the T_2-weighted MR imaging of live mice, the following parameters were adopted: spin-echo method, point resolution = 234 × 234 μm, section thickness = 2.0 mm, TE = 60 ms, TR = 3000 ms, number of acquisitions = 5. All animals were treated in accordance with the guidelines of the Animal Ethics Committee of the University of Tokyo.

2.8. Histology

The excised samples were fixed overnight in 4% paraformaldehyde and then paraffin-embedded. Embedded samples were thin sliced at 10 μm thick and then stained using an Iron Stain Kit (Muto Pure Chemicals Co., Ltd., Tokyo, Japan), based on McFadzean's protocol [15], with nuclear post-staining by 1% Safranin O. Iron staining was observed using an AX80 microscope (Olympus Corporation, Tokyo, Japan). The photographs were further quantified using Adobe Photoshop software (Adobe Systems Incorporated, San Jose, CA, USA), ImageJ software (National Institute of Health, MD, USA), and Microsoft Excel software (Microsoft Corporation, Redmond, WA, USA).

3. Results and discussion

3.1. The physicochemical properties of the PEG–PAsp-coated magnetite nanoparticle: diameter and surface polymer density

For solid tumor diagnosis, it is important to develop well-designed magnetite nanoparticles. The key physicochemical properties of magnetite nanoparticles are size, surface polymer density, and surface charge, since these characteristics can affect accumulation of magnetite nanoparticles to solid tumor. The PEG–PAsp-coated magnetite nanoparticles were prepared by mixing solutions of magnetite nanoparticles and PEG–PAsp with various molar ratios of the Asp residues to Fe (Asp/Fe); Asp/Fe ranged from 0.01 to 0.5, where [Fe] = 10 mmol/l. As seen in Fig. 1, the transmission electron microscopy (TEM) image with 75 kV accelerating voltage of nanoparticles mounted on carbon grid from aqueous solution revealed that PEG–PAsp-coated magnetite nanoparticles take a cubic shape with a mean particle diameter of approximately 10 nm. The PEG–PAsp coating was observed as a layer with a thickness of approximately 5 nm, surrounding the magnetite nanoparticles. It was also observed in the TEM image that these PEG–PAsp-coated nanoparticles form clusters with a size range of 100 nm.

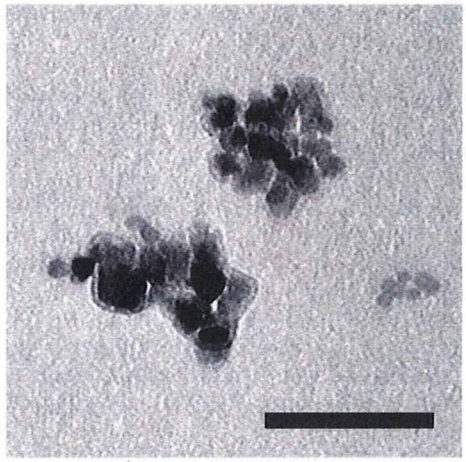

Fig. 1. TEM image of the PEG–PAsp-coated magnetite nanoparticles. Bar: 100 nm.

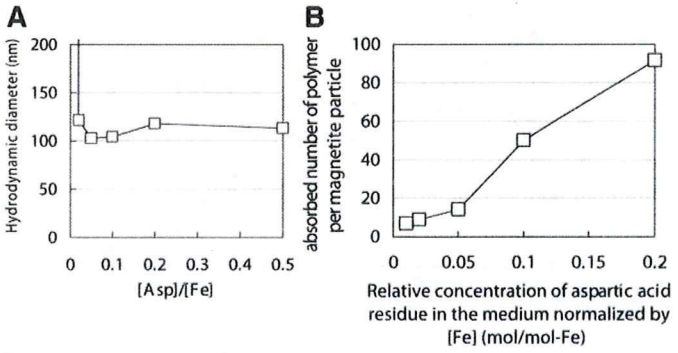

Fig. 2. Physicochemical properties of the PEG–PAsp-coated magnetite nanoparticles. (A) Hydrodynamic diameter vs. relative concentration of aspartic acid residue in the medium normalized by [Fe] (mol/mol-Fe) (=[Asp]/[Fe]), and (B) Change in the adsorbed density of PEG–PAsp on the magnetite surface estimated from TGA analysis with a bulk concentration of PEG–PAsp. Temperature = 37 °C; medium: distilled water.

The hydrodynamic diameter of these nanoparticles in aqueous medium was then measured with DLS and shown to be in the range of 100 to 120 nm with unimodal distribution, for Asp/Fe ratios ranging from 0.02–0.5. This DLS data is consistent with the cluster formation of nanoparticles indicated from TEM images. However, with a lowered Asp/Fe ratio as 0.01, the hydrodynamic diameter increased significantly (Fig. 2A). This result indicates that there is a critical surface concentration of PEG to effectively prevent the PEG–PAsp-coated magnetite nanoparticles from the agglomeration. The purified nanoparticles were stable in distilled water as 100 nm-scaled cluster at room temperature as well as at 37 °C, maintaining the initial photon count and distribution in DLS analysis for at least one month, even after the ultrafiltration to remove free PEG–PAsp possibly remained in the reactant.

The density of the PEG–PAsp block copolymer on the magnetite particle surface was estimated by TGA. Here, nanoparticles were heated in the nitrogen atmosphere to selectively vaporize the polymer fraction. Eventually, the amount of absorbed polymer on the surface of the nanoparticles was measured from the weight change by heating. The polymer density was then calculated from the TGA measurement for all the nanoparticles, assuming the cubic morphology as evidenced by microscopy and a density of 5.05 g/cm^3 for magnetite. As seen in Fig. 2B, the number of polymer strands on the nanoparticle surface was as high as 100. This data suggests that the PEG density on the magnetite nanoparticles is a little lower than that of PEGylated gold nanoparticles prepared through the surface tethering of PEG-SH [16].

3.2. The mechanism of PEG–PAsp adsorption on the magnetite nanoparticles

To confirm the formation of PEG–PAsp coating on the magnetite nanoparticles, the ζ-potential of bare and PEG–PAsp-coated magnetite nanoparticles was measured in 10 mM MOPS buffer as a function of

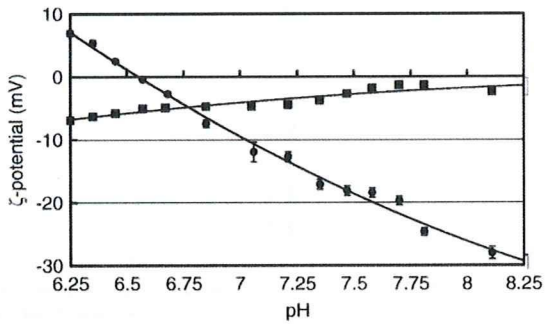

Fig. 3. Change in the ζ-potential with pH for bare (●) and PEG–PAsp-coated (■) magnetite nanoparticles. Temperature = 37 °C; medium: 10 mM MOPS buffer.

pH (Fig. 3). The isoelectric point (IEP) of the bare magnetite nanoparticles was estimated as approximately 6.6, which is consistent with the reported IEP value of iron oxide [17]. In a lower pH (below the IEP), the magnetite nanoparticle surface was protonated to result in a positive ζ-potential. Thus, in this pH range, electrostatic attraction between positively-charged magnetite nanoparticles and negatively charged PEG–PAsp is expected to occur, allowing the PEG–PAsp adsorption to the nanoparticle surface. Alternatively, the bare magnetite nanoparticles possess negative ζ-potential at physiological pH 7.4, whereas the ζ-potential shifted to the neutral value for PEG–PAsp modified nanoparticles in 10 mM MOPS buffer (pH 7.4), being consistent with the formation of a PEG shell layer. Also, these data suggest that there should be an adsorption mechanism other than simple electrostatic interaction, because magnetite has a negative ζ-potential value at pH 7.4 to induce electrostatic repulsive force against negatively charged carboxylates in PEG–PAsp. The adsorption mechanism under physiological pH was suggested to be the monodentate chelation (I) (Fig. 4) from the result of Fourier transform infrared spectroscopy [18], as explained in detail in Supplemental Text with Supplemental Fig. 1 and Supplemental Table 1.

3.3. Comparison study of the physicochemical characteristics of the PEG–PAsp- and dextran-coated magnetite nanoparticles

The MRI detection limit was compared between the PEG–PAsp- and dextran-coated magnetite nanoparticles in the field of 0.47 T at 25 °C from the relaxivity r_2, exhibiting the sensitivity of the T_2 MRI contrast agent. The dextran-coated magnetite used in this study was the one already in clinical use, Resovist®. Eventually, the relaxivity r_2 of the PEG–PAsp nanoparticle was calculated to be 138 $mM^{-1}\,s^{-1}$, the value similar to Resovist® [19].

The hydrodynamic diameter observed between the PEG–PAsp-coated and dextran-coated magnetite nanoparticles differed significantly in an NaCl-concentration-dependent manner (Fig. 5A). Although the hydrodynamic diameter of the PEG–PAsp-coated magnetite nanoparticles did not change significantly up to 3 M NaCl, indicating the appreciable stability of the PEG–PAsp-coating, that of Resovist® significantly increased even at NaCl = 0.15 M, and reached more than 1 μm at NaCl = 0.5 M, due to the drastic aggregation. Note that the PEG–PAsp-coated nanoparticles did not show any change in

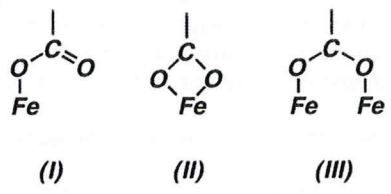

Fig. 4. Modes of carboxylate-metal complexation: monodentate (**I**), bidentate chelating (**II**), and bidentate bridging (**III**).

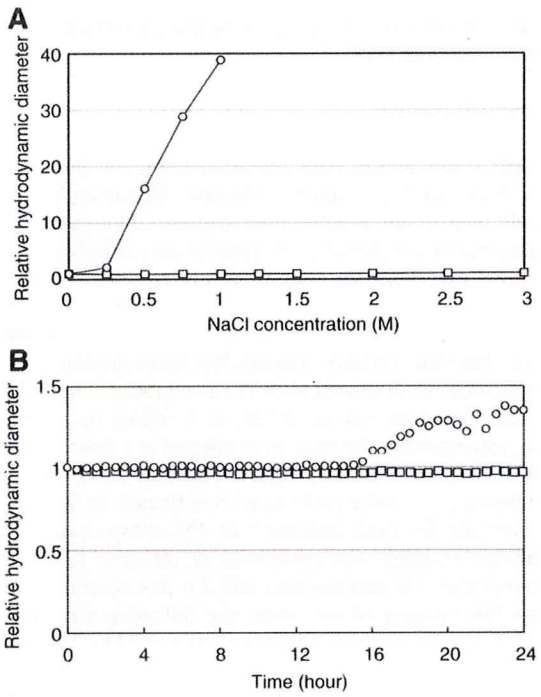

Fig. 5. NaCl concentration (A) and time (B) dependencies of the relative hydrodynamic diameter of magnetite nanoparticles, □: PEG–PAsp-coated nanoparticles, ○: dextran-coated nanoparticles (Resovist®). Fe concentration = 2 mmol/l; temperature = 37 °C; medium 10 mM Tris–HCl buffered saline (pH 7.4). 10% fetal bovine serum was contained in (B).

their size even after one month storage in 10 mM Tris–HCl buffered saline (pH 7.4, 37 °C) (data not shown).

The colloidal stability of the PEG–PAsp-coated magnetite nanoparticles in physiological conditions was also examined. We incubated them in 10 mM Tris–HCl buffered saline (pH 7.4) containing 10% fetal bovine serum at 37 °C for 24 h and measured the change of the hydrodynamic diameter (Fig. 5B). The size of the PEG–PAsp-coated magnetite nanoparticles did not obviously change during the 24-hour storage time. On the other hand, the size of Resovist® increased by the formation of aggregates after 16 h of storage time.

The stability of the PEG–PAsp-coated nanoparticles may come from the multivalent bonding between flanking carboxylic groups and the magnetite surface, as suggested by FT-IR study. These findings are consistent with a report showing that PEG-oligo(aspartic acid) block copolymer-coated iron oxide nanoparticles were stable at pH 2–11 and in 1 M NaCl, where the repeating number of aspartic acid units was 3 or more [20]. In contrast, instability of Resovist® against salt addition may be due to weak interaction between magnetite and hydroxyl groups of dextran [21].

3.4. MR imaging of experimental pancreatic cancer in vivo

The MR imaging of tumor tissue *in vivo* was then conducted by comparing PEG–PAsp- and dextran-coated magnetite nanoparticles, Resovist®. Resovist® has already been approved for clinical use as a liver-specific MRI contrast agent, due to accumulation into the reticuloendothelial system (RES) of the normal liver. Most malignant liver tumors do not contain RES cells and therefore are contrasted positive by Resovist®. A xenografted BxPC3 human pancreatic adenocarcinoma cell line in nude mice, characterized histologically by fibrosis and hypovascularity, was used as a model of intractable cancer. Recently, we reported that the administration of TGF-β inhibitor to tumor model mice significantly enhanced the intratumoral accumulation of nanoparticles encapsulating anticancer drugs [11]. Thus, we tested the effect of the i.p. administration of TGF-β

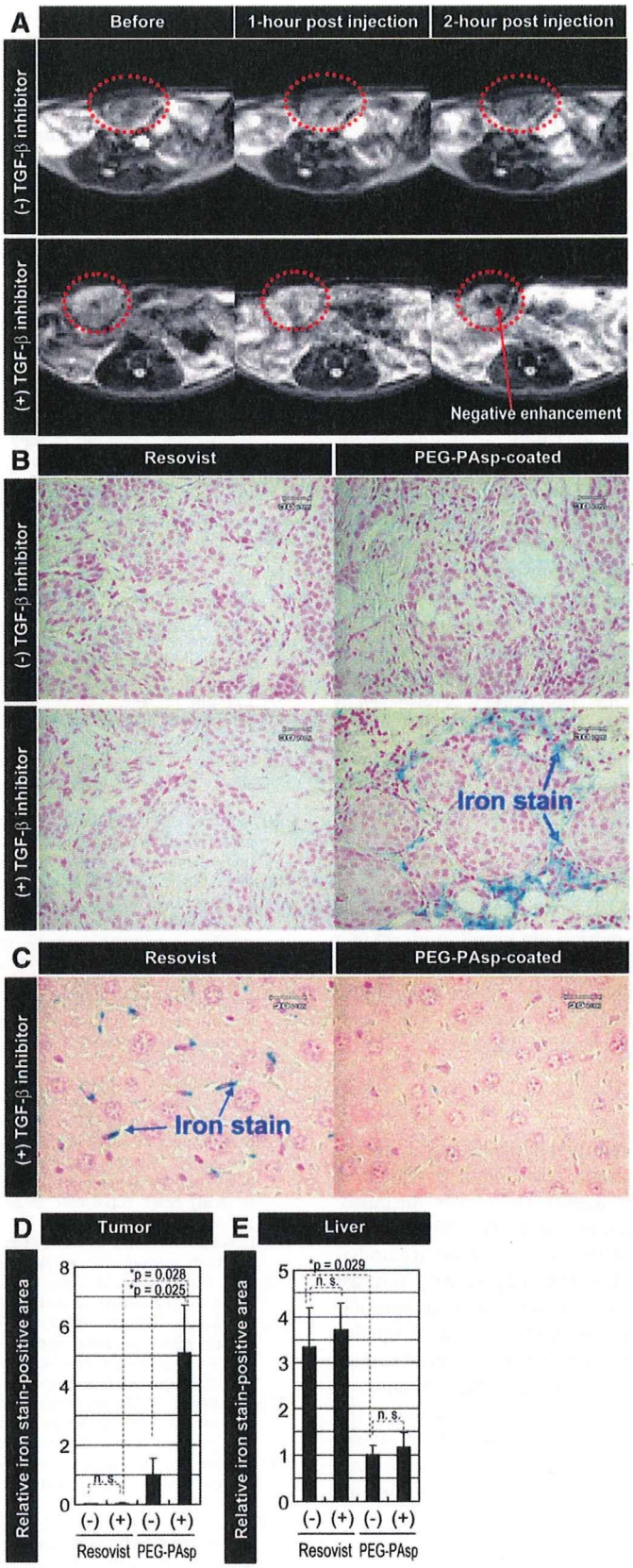

Fig. 6. MR imaging of experimental pancreatic cancer *in vivo* and the distribution of the nanoparticles in cancer and liver tissues. (A) T_2-weighted images of tumor-implanted mice (tumor sites are circled by red dotted line) at different temporal points after injection of PEG–PAsp-coated magnetite nanoparticles and TGF-β inhibitor. All images were obtained in a field strength of 4.7 T. (B) Histological sections of BxPC3 xenograft stained with Prussian blue. The distribution of Resovist® and PEG–PAsp-coated magnetite nanoparticles, at 5.5 mg/kg with and without TGF-β inhibitor at 1 mg/kg, were examined 24 h after the administration. (C) Histological sections of liver stained with Prussian blue. The distribution of Resovist® and PEG–PAsp-coated magnetite nanoparticles, at 5.5 mg/kg with TGF-β inhibitor at 1 mg/kg, was examined 24 h after the administration. (D and E) Areas of iron staining in the tumor and liver were quantified. PEG–PAsp, PEG–PAsp coated magnetite nanoparticles with (+) and without (−) inhibitor. Error bars in the graphs represent standard errors of the mean ($n = 6$), and P values were calculated by two-tailed Student's t test. n.s.: not significant.

inhibitor with the i.v. administration of Resovist® or the PEG–PAsp-coated magnetite nanoparticles on their imaging capability in size-matched xenografts of the BxPC3 cell line. Fig. 6A shows the T_2-weighted MR images of the tumors at different time periods after the intravenous administration (preinjection, and 1 and 2 h postinjection) of PEG–PAsp-coated magnetite nanoparticles with and without TGF-β inhibitor.

Resovist® failed to image the tumor even with the co-administration of TGF-β inhibitor, presumably due to the non-specific accumulation into the reticuloendothelial system [8]. In contrast, the PEG–PAsp-coated magnetite nanoparticles exhibited significant negative enhancement of signal intensity in the tumor region of T_2-weighted images when combined with TGF-β inhibitor, suggesting the accumulation of detectable amounts of the PEG–PAsp-coated magnetite nanoparticles within 2 h after injection. Therefore, the difference in behavior of these two types of magnetite nanoparticles *in vivo* had a crucial importance in achieving effective tumor accumulation for successful MR imaging.

To further verify the accumulation of iron oxide nanoparticles in the tumor, we performed Prussian blue staining of the tumor tissues to detect iron oxide, which stains blue. As shown in Fig. 6B, positive staining of the tumor for iron oxide was only obvious in the condition with PEG–PAsp-coated nanoparticles combined with the TGF-β inhibitor. Areas of iron staining in the tumor were then quantified as seen in Fig. 6D, demonstrating a significant increase in the areas of positive staining by TGF-β inhibitor treatment. The presence of iron oxide was consistent with the MRI results. Iron oxide was observed in the area rich in fibrotic components, suggesting that the administration of TGF-β inhibitor transiently increases the permeability of the tumor capillary to promote the extravasation of the PEG–PAsp-coated magnetite nanoparticles, even though the BxPC3 tumor has the characteristic of hypovascularity [11].

Lastly, we examined liver tissues from the mice treated with Resovist® or the PEG–PAsp-coated magnetite nanoparticle, with or without TGF-β inhibitor, by iron staining (Fig. 6C). Although aggregates of Resovist® accumulated in the liver, particularly in cells with smaller nuclei (presumably Kuppfer cells), far less PEG–PAsp-coated magnetite nanoparticles accumulated in the liver without aggregation. These results did not differ with or without TGF-β inhibitor, which was determined by the area of Prussian blue staining (Fig. 6E).

4. Conclusion

In conclusion, we here demonstrated the physicochemical properties of PEG–PAsp-coated magnetite nanoparticles and the feasibility of these nanoparticles as MR contrast agents for cancer diagnosis. Improving the stability of nanoparticles might be important for enabling a longer half-life in the bloodstream and a better accumulation in tumor tissue, leading to effective MR imaging with contrast agents. The neutral ζ-potential of the PEG–PAsp-coated nanoparticle may contribute to avoidance of reticuloendothelial system uptake. Formation of the stable and dense PEG layer on the magnetite surface through the anchoring of PEG–PAsp by the monodentate chelation of COO^- residues to iron atoms definitely plays a substantial role in the increased stability of the nanoparticles *in vivo*. The use of PEG–PAsp-coated magnetite nanoparticles combined with a TGF-β inhibitor could thus become a novel regime in the diagnosis of intractable cancers, including pancreatic adenocarcinoma.

Acknowledgements

The authors thank Dr James R. Christie II, The University of Tokyo, for editing the English of the manuscript. This work was supported by a Grant-in-Aid for Scientific Research from the Ministry of Education, Culture, Sports, Science and Technology (MEXT), Core Research for Evolution of Science and Technology (CREST), Japan Science and Technology Corporation (JST), and the 21st century COE program 'Human-Friendly Materials based on Chemistry' from MEXT.

Appendix A. Supplementary data

Supplementary data associated with this article can be found, in the online version, at doi:10.1016/j.jconrel.2009.06.002.

References

[1] M.R. Dreher, W. Liu, C.R. Michelich, M.W. Dewhirst, F. Yuan, A. Chilkoti, Tumor vascular permeability, accumulation, and penetration of macromolecular drug carriers, J. Natl. Cancer Inst. 98 (5) (2006) 335–344.
[2] H.A. Burris, M.J. Moore, J. Andersen, M.R. Green, M.L. Rothenberg, M.R. Modiano, M.C. Cripps, R.K. Portenoy, A.M. Storniolo, P. Tarassoff, R. Nelson, F.A. Dorr, C.D. Stephens, D.D. Von Hoff, Improvements in survival and clinical benefit with gemcitabine as first-line therapy for patients with advanced pancreas cancer: a randomized trial, J. Clin. Oncol. 15 (6) (1997) 2403–2413.
[3] D.V. Sahani, Z.K. Shah, O.A. Catalano, G.W. Boland, W.R. Brugge, Radiology of pancreatic adenocarcinoma: current status of imaging, J. Gastroenterol. Hepatol. 23 (1) (2008) 23–33.
[4] D.L. Huber, Synthesis, properties, and applications of iron nanoparticles, Small 1 (5) (2005) 482–501.
[5] R. Weissleder, G. Elidonzo, J. Wittenberg, C.A. Rabito, H.H. Bengele, L. Josephson, Ultrasmall superparamagnetic iron oxide: characterization of a new class of contrast agents for MR imaging, Radiology 175 (2) (1990) 489–493.
[6] M. Lewin, N. Carlesso, C.H. Tung, X.W. Tang, D. Cory, D.T. Scadden, R. Weissleder, Tat peptide-derivatized magnetic nanoparticles allow *in vivo* tracking and recovery of progenitor cells, Nat. Biotechnol. 18 (4) (2000) 410–414.
[7] Y.W. Jun, J.H. Lee, J. Cheon, Chemical design of nanoparticle probes for high-performance magnetic resonance imaging, Angew. Chem. Int. Ed. 47 (28) (2008) 5122–5135.
[8] D.D. Stark, R. Weissleder, G. Elizondo, et al., Superparamagnetic iron oxide: clinical application as a contrast agent for MR imaging of the liver, Radiology 168 (2) (1988) 297–301.
[9] T. Neuberger, B. Schöpf, H. Hofmann, M. Hofmann, B. von Rechenberg, Superparamagnetic nanoparticles for biomedical applications: possibilities and limitations of a new drug delivery system, J. Magn. Mater. 293 (1) (2005) 483–496.
[10] M. Kumagai, Y. Imai, T. Nakamura, Y. Yamasaki, M. Sekino, S. Ueno, K. Hanaoka, K. Kikuchi, T. Nagano, E. Kaneko, K. Shimokado, K. Kataoka, Iron hydroxide nanoparticles coated with poly(ethylene glycol)–poly(aspartic acid) block copolymer as novel magnetic resonance contrast agents for *in vivo* cancer imaging, Colloids Surf. B: Biointerfaces 56 (1–2) (2007) 174–181.
[11] M.R. Kano, Y. Bae, C. Iwata, Y. Morishita, M. Yashiro, M. Oka, T. Fujii, A. Komuro, K. Kiyono, M. Kaminishi, K. Hirakawa, Y. Ouchi, N. Nishiyama, K. Kataoka, K. Miyazono, Improvement of cancer-targeting therapy, using nanocarriers for intractable solid tumors by inhibition of TGF-β signaling, Proc. Natl. Acad. Sci. U. S. A. 104 (9) (2007) 3460–3465.
[12] Y. Matsumura, H. Maeda, A new concept for macromolecular therapeutics in cancer-chemotherapy-mechanism of tumoritropic accumulation of proteins and the antitumor agent SMANCS, Cancer Res. 46 (12) (1986) 6387–6392.
[13] N. Nishiyama, M. Yokoyama, T. Aoyagi, T. Okano, Y. Sakurai, K. Kataoka, Preparation and characterization of self-assembled polymer-metal complex micelle from cis-dichlorodiammineplatinum(II) and poly(ethylene glycol)–poly(alpha,beta-aspartic acid) block copolymer in an aqueous medium, Langmuir 15 (2) (1999) 377–383.
[14] E. Fukushima, S.B.W. Roeder (Eds.), Experimental pulse NMR: a nuts and bolts approach, Addison-Wesley, Reading, Mass, 1981, pp. 28–35.
[15] A.J.S. MacFadzean, L.J. Davis, Iron-staining erythrocytic inclusions with especial reference to acquired haemolytic anaemia, Glasgow Med. J. 28 (1947) 237–279.
[16] S. Takae, Y. Akiyama, H. Otsuka, T. Nakamura, Y. Nagasaki, K. Kataoka, Ligand density effect on biorecognition by PEGylated gold nanoparticles: regulated interaction of RCA120 lectin with lactose installed to the distal end of tethered PEG strands on gold surface, Biomacromolecules 6 (2) (2005) 818–824.
[17] L. Cromières, V. Moulin, B. Fourest, E. Giffaut, Physico-chemical characterization of the colloidal hematite/water interface: experimentation and modeling, Colloids Surf., A. Physicochem. Eng. Asp. 202 (1) (2002) 101–115.
[18] L.J. Kirwan, P.D. Fawell, W. van Bronswijk, In situ FTIR-ATR examination of poly (acrylic acid) adsorbed onto hematite at low pH, Langmuir 19 (14) (2003) 5802–5807.
[19] Y.X.J. Wang, S.M. Hussain, G.P. Krestin, Superparamagnetic iron oxide contrast agents: physicochemical characteristics and applications in MR imaging, Eur. Radiol. 11 (11) (2001) 2319–2331.
[20] S.R. Wan, J.S. Huang, M. Guo, H. Zhang, Y. Cao, H. Yan, K. Liuet, Biocompatible superparamagnetic iron oxide nanoparticle dispersions stabilized with poly (ethylene glycol)oligo(aspartic acid) hybrids, J. Biomed. Mater. Res. A 80A (4) (2007) 946–954.
[21] C.W. Jung, Surface-properties of superparamagnetic iron-oxide MR contrast agents — ferumoxides, ferumoxtran, ferumoxsil, Magn. Reson. Imaging 13 (5) (1995) 675–691.

Enhanced Percolation and Gene Expression in Tumor Hypoxia by PEGylated Polyplex Micelles

Muri Han[1], Makoto Oba[2], Nobuhiro Nishiyama[3,4], Mitsunobu R Kano[4,5], Shinae Kizaka-Kondoh[6] and Kazunori Kataoka[1,3,4,7]

[1]Department of Materials Engineering, Graduate School of Engineering, The University of Tokyo, Tokyo, Japan; [2]Department of Clinical Vascular Regeneration, Graduate School of Medicine, The University of Tokyo, Tokyo, Japan; [3]Center for Disease Biology and Integrative Medicine, Graduate School of Medicine, The University of Tokyo, Tokyo, Japan; [4]Center for NanoBio Integration, The University of Tokyo, Tokyo, Japan; [5]Department of Molecular Pathology, Graduate School of Medicine, The University of Tokyo, Tokyo, Japan; [6]Department of Radiation Oncology and Image-Applied Therapy, Kyoto University, Graduate School of Medicine, Kyoto, Japan; [7]Core Research for Evolutional Science and Technology (CREST), Japan Science and Technology Agency (JST), Kawaguchi, Japan

In regard to gene vectors for cancer gene therapy, their percolation into the tumor tissue should be essential for successful outcome. Here, we studied the tumor penetrability of nonviral vectors (polyplexes) after incubation with the multicellular tumor spheroid (MCTS) models and intratumoral (i.t.) injection into subcutaneous tumors. As a result, polyethylene glycolated (PEGylated), core–shell type polyplexes (polyplex micelles) showed facilitated percolation and improved transfection inside the tumor tissue, whereas conventional polyplexes from cationic polymers exhibited limited percolation and localized transfection. Furthermore, the transfection of hypoxia-responsive plasmid demonstrated that polyplex micelles allowed the transfection to the hypoxic region of the tumor tissue in both *in vitro* and *in vivo* experiments. To the best of our knowledge, our results demonstrated for the first time that polyplex micelles might show improved tumor penetrability over cationic polyplexes, thereby achieving transfection into the inside of the tumor tissue.

Received 22 December 2008; accepted 24 April 2009; published online 26 May 2009. doi:10.1038/mt.2009.119

INTRODUCTION

Gene therapy is a promising method for the treatment of malignant tumors, and its success relies on the capabilities of gene vectors. In this regard, nonviral vectors composed of plasmid DNA (pDNA) and cationic polymers, so-called polyplexes have been attracting much attention due to several advantages such as no immunogenicity, safety, and easy large-scale preparation.[1–4] So far, considerable efforts have been devoted to improve the transfection efficiency of polyplexes as well as control the gene expression in the body.[5–8] However, in regard to gene vectors for cancer gene therapy, much attention should be paid on another important property: percolation into the tumor tissue. In general, solid tumors are known to possess heterogeneous structures composed of blood vessels, interstitial tissues, clusters of tumor cells with normoxic and hypoxic regions. Therefore, it might be difficult to deliver the therapeutic agents to tumor cells distant from the vasculature.[9–11] Furthermore, hypoxic region induced by the insufficient blood supply is known to be inherently less susceptible to therapeutic agents.[10] As such difficulty in treating hypoxic regions is often correlated with recurrence and malignant progression of solid tumors,[10] overcoming the limited drug access to hypoxic cells should be a critical issue in cancer therapy. Thus, the percolation of gene vectors in solid tumors should be of primary importance to achieve successful cancer gene therapy.

Recently, we have developed a highly transfectable but less-toxic core–shell type polyplex with poly(ethylene glycol) (PEG) palisades (polyplex micelle), which was formed through the electrostatic interaction between pDNA and PEG-*b*-polyaspartamide having 1,2-diaminoethane side chain (PEG-*b*-P[Asp(DET)]) (**Figure 1**).[12,13] This polyplex micelle showed remarkable features, including efficient gene transfer to primary cells,[12] successful *in vivo* transfection to a rabbit carotid artery,[14] and transfection-mediated bone regeneration.[15] In this study, we explored the tumor penetrability of polyplex micelles, because we have recently demonstrated that amphiphilic block copolymer micelles can show penetrability into multicellular tumor spheroids (MCTSs)[16] as well as solid tumors after intravenous administration.[17] Here, we demonstrated that polyplex micelles from PEG-*b*-P[Asp(DET)] showed successful transfection to hypoxic cells inside MCTS as well as enhanced percolation and widely distributed gene expression within the tumor tissue after intratumoral (i.t.) injection. In contrast, cationic polyplexes showed limited penetration and localized transfection in both *in vitro* and *in vivo* studies. These results suggest that polyplex micelles may overcome the transport barrier of nonviral vectors, facilitating their use for cancer gene therapy.

RESULTS

Transfection to MCTS

MCTS is an appropriate *in vitro* tumor model representing morphological and functional features of *in vivo* avascular solid tumors, and is composed of actively proliferating outer cell layers

Correspondence: *Kazunori Kataoka, Department of Materials Engineering, Graduate School of Engineering, The University of Tokyo, 7-3-1 Hongo, Bunkyo-ku, Tokyo 113-8656, Japan. E-mail: kataoka@bmw.t.u-tokyo.ac.jp*

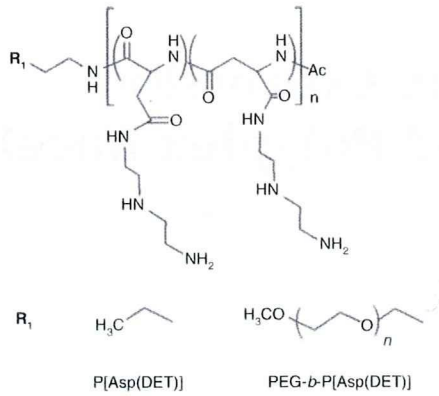

Figure 1 Chemical structures of P[Asp(DET)] homopolymers and PEG-*b*-P[Asp(DET)] block copolymers.

and hypoxic and quiescent inner cells.[18] In this study, a large-sized MCTS (400–500 μm), which possessed a hypoxic region characterized by necrotic cells inside due to limited supply of oxygen and nutrition (**Figure 2a**), was transfected with pCAcc + *Venus* by using the linear polyethylenimine (LPEI) and P[Asp(DET)] polyplexes and PEG-*b*-P[Asp(DET)] polyplex micelles at a defined mixing ratio of the number of amino groups units to a nucleotide unit (N/P ratio). Note that, although we have recently reported that a small-sized MCTS (~100 μm) can be disrupted by the cytotoxicity of polyplexes,[19] the large-sized MCTS used in this study is stable against the polyplex-mediated transfection. The expression of a variant of yellow fluorescent protein, *Venus* was evaluated by confocal microscopic observation. At 48 hours after the transfection (24-hour incubation and additional 24-hour incubation after the medium replacement), the LPEI polyplexes (N/P = 6, the manufacturer's recommendation ratio) and P[Asp(DET)] polyplexes (N/P = 20) showed significant gene expression limited to the periphery of the MCTS (**Figure 2b**). This result indicates that cationic polyplexes might lack the ability to transfect the inside of the MCTS. In contrast, PEG-*b*-P[Asp(DET)] polyplex micelles (N/P = 20) showed appreciable gene expression at not only the periphery but also the inside of the MCTS (**Figure 2b**), where a great number of necrotic cells were observed as indicated by red fluorescence from ethidium homodimer (EthD-1) (**Figure 2c**). These results suggest that polyplex micelles may allow the gene transfer to tumor cells in the hypoxic inner region of the MCTS.

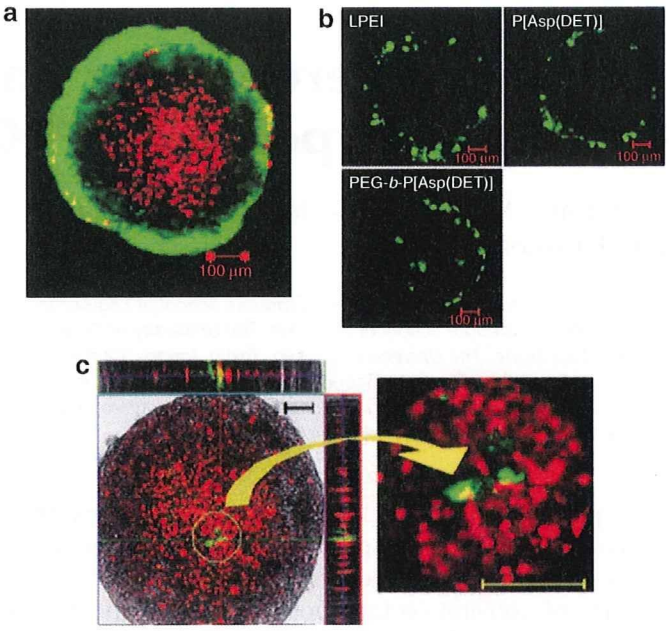

Figure 2 Transfection to HuH-7 MCTS. (**a**) Live/dead staining of HuH-7 spheroid (optical slice at the middle of spheroid. Bar = 100 μm). The green and red fluorescence are derived from live and dead cells, respectively. (**b**) Gene expression of pCAcc + *Venus* in HuH-7 MCTS transfected with LPEI polyplexes (N/P = 6), P[Asp(DET)] polyplexes (N/P = 20), and PEG-*b*-P[Asp(DET)] polyplex micelles (N/P = 20) (24 hours of incubation time and 24 hours of additional incubation after the medium replacement). (**c**) Gene expression of pCAcc + *Venus* at the inner region of HuH-7 MCTS transfected with PEG-*b*-P[Asp(DET)] polyplex micelles (N/P = 20) (24 hours of incubation time and 24 hours of additional incubation after the medium replacement) (Left: The red and green fluorescence are derived from dead cells and transfected protein *Venus*, respectively. Right: Magnified image of the circled region in the left picture). LPEI, linear polyethylenimine; MCTS, multicellular tumor spheroid; N/P, ratio of the number of amino groups units to a nucleotide unit.

Hypoxia-selective gene expression in the MCTS

To confirm the gene expression in hypoxic cells in the MCTS, we carried out the transfection study using pDNA encoding *Venus* driven by the 5× hypoxia-responsive element (5HRE) promoter (p5HRE + *Venus*). The hypoxia-selectivity of p5HRE + *Venus* was examined in monolayer cultured HuH-7 cells under hypoxic conditions reproduced by iron-chelating agent, deferoxamine mesylate.[20] As shown in **Figure 3a**, PEG-*b*-P[Asp(DET)] polyplex micelles containing hypoxia-responsive p5HRE + *Venus* showed no gene expression under normoxic conditions (0 μmol/l deferoxamine mesylate) but an appreciable gene expression under hypoxia-mimicking conditions (200 μmol/l deferoxamine mesylate). Note that polyplex micelles containing hypoxia-irresponsive pCAcc + *Venus* exhibited significant gene expression under both normoxic and hypoxic conditions. Thus, p5HRE + *Venus* was demonstrated to be highly selective to hypoxic environments. Then, LPEI and P[Asp(DET)] polyplexes and PEG-*b*-P[Asp(DET)] polyplex micelles containing p5HRE + *Venus* were applied to the transfection to the large-sized MCTS (400–500 μm). As a result, none of 5 spheroids transfected with LPEI polyplexes showed the expression of p5HRE + *Venus* (data not shown), which may be consistent with the expression of pCAcc + *Venus* limited to the periphery of the MCTS (**Figure 2b**). Surprisingly, P[Asp(DET)] polyplexes exhibited the expression of p5HRE + *Venus* in two of five spheroids at 48 hours after the transfection; however, the gene expression was limited to the outer rims of hypoxic regions at ~100 μm distance from the periphery of the MCTS (**Figure 3b**; the yellow circle is the initial size of spheroids before the transfection). This result suggests that P[Asp(DET)] polyplexes could penetrate into the inside of the spheroids to some extent. In contrast, PEG-*b*-P[Asp(DET)] polyplex micelles allowed the transfection of p5HRE + *Venus* to a larger number of the cells in the inner region of the MCTS in 7 of 10 spheroids (**Figure 3b**), suggesting the ability of the polyplex micelles to transfect hypoxic cells inside of the spheroids. To further confirm this effect, two distinct plasmids encoding DsRedC1 (red fluorescence) driven

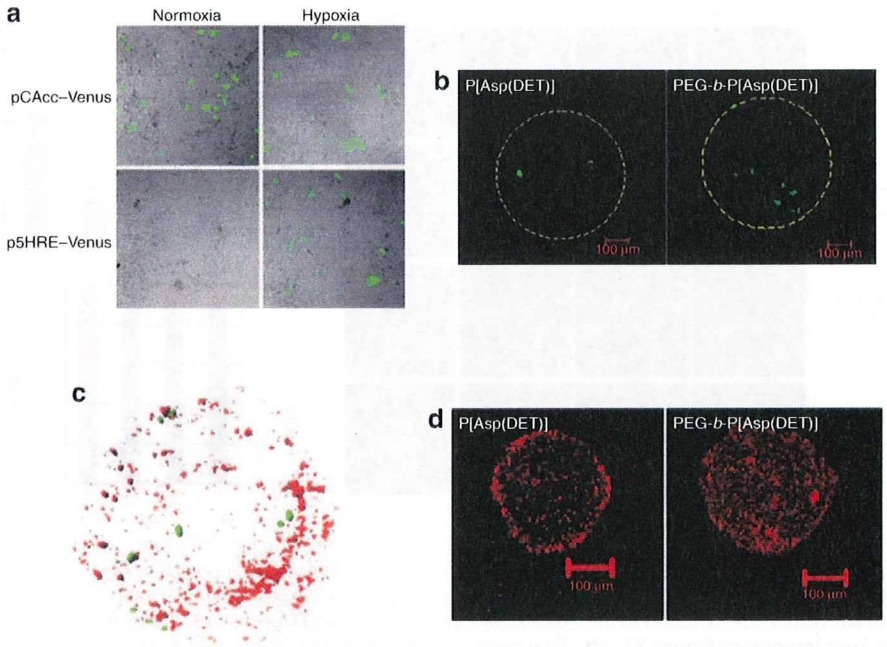

Figure 3 Hypoxia selective gene expression in the MCTS. (**a**) Gene expressions of hypoxia-irresponsive pCAcc + *Venus* and hypoxia-responsive p5HRE + *Venus* in monolayer cultured HuH-7 cells under normoxic and hypoxic conditions. HuH-7 cells were incubated with PEG-*b*-P[Asp(DET)] polyplex micelles (N/P = 20) for 24 hours, followed by additional 24 hours incubation after the medium replacement. Hypoxia-mimicking conditions were reproduced by incubating the cells with iron chelating agent, DFx during the postincubation. (**b**) Gene expressions of hypoxia-responsive p5HRE + *Venus* in the HuH-7 spheroids transfected with P[Asp(DET)] polyplexes and PEG-*b*-P[Asp(DET)] polyplex micelles (N/P = 20). The yellow circle indicates the size of the MCTS at the time of the transfection. (**c**) Piled up images of the gene expressions of hypoxia-irresponsive pCMV-DsRedC1 (red fluorescence) and hypoxia-responsive p5HRE – *Venus* (green fluorescence) in the MCTS transfected with PEG-*b*-P[Asp(DET)] polyplex micelles incorporating each plasmid (N/P = 20). (**d**) Distribution of Cy3-labeled pDNA encapsulated into P[Asp(DET)] polyplexes (N/P = 20) and PEG-*b*-P[Asp(DET)] polyplex micelles (N/P = 20) in HuH-7 MCTS after 24-hour incubation. The images were taken at the center of the spheroids. DFx, deferoxamine mesylate; MCTS, multicellular tumor spheroid; N/P, ratio of the number of amino groups units to a nucleotide unit.

by the cytomegalovirus (CMV) promoter (pCMV-DsRedC1) and *Venus* (green fluorescence) driven by the 5HRE promoter (p5HRE – *Venus*) were independently encapsulated into PEG-*b*-P[Asp(DET)] polyplex micelles, and then applied to the transfection to the MCTS. After 48 hours, optical slices of the MCTS at a depth of 1 μm were taken by confocal microscopy, and then piled up by Imaris software (Carl Zeiss, Jena, Germany) to obtain the three-dimensional localization of each fluorescence. As shown in **Figure 3c**, the expression of p5HRE – *Venus* was mainly detected in the inner region of the MCTS, whereas the expression of pCMV-DsRedC1 was observed throughout the MCTS. Thus, the hypoxic inner regions of the MCTS were successfully transfected with PEG-*b*-P[Asp(DET)] polyplex micelles.

Percolation of polyplexes and polyplex micelles into the MCTS

The percolation of the polyplexes and polyplex micelles into the MCTS was investigated by using Cy3-labeled pDNA. In this study, the MCTS with a diameter of 200–250 μm was used to detect weak fluorescence from Cy3-labeled pDNA within the spheroids. **Figure 3d** shows the fluorescent image of Cy3-labeled pDNA at the center of HuH-7 MCTS after 24-hour incubation with polyplexes or polyplex micelles. Note that the treatment of the relatively small-sized MCTS with LPEI polyplexes resulted in destruction of spheroid structures due to the cytotoxicity of LPEI as previously reported.[19] As shown in **Figure 3d**, P[Asp(DET)] polyplexes displayed apparent fluorescence at the periphery of spheroids. This result is consistent with the previous report that cationic polyplexes could penetrate only the outer 3–5 proliferating cell layers (10–20 μm) of the MCTS.[11] In contrast, the pDNA formulated in PEG-*b*-P[Asp(DET)] polyplex micelles showed well-distributed fluorescence within spheroids, suggesting their percolation into the inside of the spheroids. Similar results were obtained when the MCTS model from a different cell line (*i.e.*, human pancreatic BxPC3 cells) were used (**Supplementary Figure S1**). Thus, polyplex micelles might possess the ability to percolate into the spheroids over cationic polyplexes.

i.t. distribution of polyplexes and polyplex micelles after i.t. injection

The i.t. distribution of naked pDNA, LPEI polyplexes (N/P = 6), P[Asp(DET)] polyplexes (N/P = 20), or PEG-*b*-P[Asp(DET)] polyplex micelles (N/P = 20) after the injection to solid tumors (human pancreatic adenocarcinoma BxPC3 cells) was evaluated by using Cy3-labeled pDNA (n = 3). In this experiment, each formulation was coadministered with FluoSphere fluorescent microspheres [particle size: 15 μm, 645 nm/680 nm (Ex/Em)] as a marker for the injection point. The fluorescent images of Cy3-labeled pDNA in BxPC3 tumors are shown in **Figure 4a** and **Supplementary Figure S2**, and the total pixels of fluorescence area and its localization in the three different regions classified by the distance from the injection point (<100 μm, 100–200 μm, >200 μm) are quantified